

A new perspective on flux and slope limiting in discontinuous Galerkin methods for hyperbolic conservation laws

Dmitri Kuzmin

*Institute of Applied Mathematics (LS III), TU Dortmund University
Vogelpothsweg 87, D-44227 Dortmund, Germany*

Abstract

In this work, we discuss and develop multidimensional limiting techniques for discontinuous Galerkin (DG) discretizations of scalar hyperbolic problems. To ensure that each cell average satisfies a local discrete maximum principle (DMP), we impose inequality constraints on the local Lax-Friedrichs fluxes of a piecewise-linear (\mathbb{P}_1) approximation. Since the piecewise-constant (\mathbb{P}_0) version corresponds to a property-preserving low-order finite volume method, the validity of DMP conditions can always be enforced using slope and/or flux limiters. We show that the (currently rather uncommon) use of direct flux limiting makes it possible to construct more accurate DMP-satisfying approximations in which a weak form of slope limiting is used to prevent unbounded growth of solution gradients. Moreover, both fluxes and slopes can be limited in a manner which produces nonlinear problems with well-defined residuals even at steady state. We derive/present slope limiters based on different kinds of inequality constraints, discuss their properties and introduce new anisotropic limiters for problems that require different treatment of different space directions. At the flux limiting stage, the anisotropy of the problem at hand can be taken into account by using a customized definition of local bounds for the DMP constraints. At the slope limiting stage, we adjust the magnitude of individual directional derivatives using low-order reconstructions from cell averages to define the bounds. In this way, we avoid unnecessary limiting of well-resolved derivatives at smooth peaks and in internal/boundary layers. The properties of selected algorithms are explored in numerical studies for DG- \mathbb{P}_1 discretizations of two-dimensional test problems. In the context of *hp*-adaptive DG methods, the new limiting procedures can be used in \mathbb{P}_1 subcells of macroelements marked as ‘troubled’ by a smoothness indicator.

Keywords: hyperbolic conservation laws, discrete maximum principles, positivity preservation, discontinuous Galerkin methods, flux correction, slope limiting

1. Introduction

Discontinuous Galerkin (DG) belong to the family of discretization techniques in which the evolution of cell averages and their values at steady state are determined by the choice of numerical fluxes. The

Email address: kuzmin@math.uni-dortmund.de (Dmitri Kuzmin)

commonly employed local Lax Friedrichs (LLF) flux approximation provably guarantees the validity of local discrete maximum principles (DMP), preservation of invariant domains, and entropy stability for piecewise-constant (\mathbb{P}_0) discretizations which are equivalent to cell-centered finite volume schemes. The LLF flux of a piecewise-linear (\mathbb{P}_1) or higher order approximation may fail to satisfy the inequality constraints that provide sufficient conditions for a DG method to possess the above properties. As a consequence, the cell averages may attain unacceptable values or violate entropy conditions.

The DMP property of a LLF flux depending on the cell averages and slopes of the DG solution in two adjacent elements can be enforced by using some form of flux and/or slope limiting. The differences between the two kinds of limiting techniques are subtle and require further explanation:

- A *flux limiter* is an algorithm which produces a convex combination of numerical fluxes corresponding to a property-preserving low-order scheme and a high-order target discretization that may violate the DMP conditions. Classical representatives of high-resolution finite volume schemes equipped with such limiters include flux-corrected transport (FCT) algorithms [5, 46] and total variation diminishing (TVD) methods [22, 23] for structured grids, as well as local extremum diminishing (LED) schemes for unstructured meshes [3, 25, 26]. Examples of bound-preserving (BP) flux limiters for \mathbb{P}_0 components of DG solutions can be found in [11, 31, 44].
- A *slope limiter* is an postprocessing tool which adjusts the derivatives of a piecewise-polynomial solution without changing the cell averages. The outcome of slope limiting is a convex combination of the \mathbb{P}_0 and \mathbb{P}_1 approximations in each cell. Many limiting techniques of this kind were proposed in the literature on finite volume and DG methods [2, 9, 12, 24, 27, 30, 48, 49]. Most of them constrain the range of values that the DG solution may attain at certain control points on the boundaries of mesh elements. This limiting criterion provides safer input data for calculation of numerical fluxes but, as noticed in [44], is generally insufficient to ensure the DMP property of the cell averages that define the local bounds for the inequality constraints of the slope limiting procedure. Hence, the resulting solutions may exhibit undershoots/overshoots.

In light of the above, slope limiting can be interpreted as indirect flux limiting via imposition of inequality constraints on the Riemann data. If the LLF flux function is linear, a convex combination of the \mathbb{P}_0 and \mathbb{P}_1 fluxes equals the flux corresponding to the convex combination of the \mathbb{P}_0 and \mathbb{P}_1 states. For linear advection in 1D, any flux limiter is equivalent to a slope limiter and vice versa [38, 47]. The design of a slope limiter which ensures the DMP property of cell averages for a general conservation law is more involved [12, 13]. Many existing slope limiters are not BP in this sense and/or may fail to preserve well-resolved directional derivatives of the DG- \mathbb{P}_1 solution. In applications to large-scale ocean flow models, the latter side effect gives rise to spurious diapycnal mixing [6, 15] and unnecessary cancellation of all partial derivatives in boundary elements. The use of anisotropic slope limiters [1, 24, 43] may alleviate these problems but does not guarantee the BP property.

The poor performance of slope limiters in applications to some anisotropic transport problems can be attributed to the fact that a steep gradient does not produce a large flux across a surface which is (almost) parallel to the flow direction. It is generally difficult to find an optimal correction factor for each derivative using inequality constraints for solution values at control points and to find the

least restrictive local bounds which guarantee the DMP property in the absence of flux limiting. On the other hand, some control of solution gradients is required even in DG schemes equipped with flux limiters [11, 44]. In contrast to finite volume schemes, the difference between the unlimited gradients of a DG- \mathbb{P}_1 approximation and a suitable reconstruction from BP cell averages may become arbitrarily large. The application of a flux limiter would prevent any violation of local bounds but the resulting approximations may turn out too diffusive or exhibit strong ‘terracing’ effects, i.e., spurious distortions within the range of values satisfying the DMP constraints. Hence, some slope limiting is still required to ensure consistency and stability of the DG approximation to the gradient but these basic requirements are far less restrictive than inequality constraints for pointwise solution values.

The methodology that we favor in the present paper combines a flux limiter based on inequality constraints for the cell averages and a slope limiter based on inequality constraints for the gradients or directional derivatives of the DG solution. The main burden of enforcing the DMP conditions falls on the flux limiter, while slope limiting provides a complementary correction tool that may be applied less frequently. This unconventional design philosophy distinguishes our new limiting strategy from mainstream approaches which either assume the BP property of the cell averages or enforce it using more sophisticated slope limiters than those that we use to control the solution gradients.

The remainder of this paper is organized as follows. In Section 2, we discretize a generic scalar conservation law in space using a DG- \mathbb{P}_1 method, formulate the DMP constraints, and discuss the definition of local bounds for anisotropic transport problems. In Section 3, we review two approaches for enforcing the corresponding inequality constraints in the process of flux limiting. The first one is based on a localized FCT algorithm (cf. [10, 16, 42]). The second type of flux correction is based on the concept of monolithic convex limiting for general finite element approximations [31, 32, 33, 34]. In Section 4, we present new slope limiters which also guarantee the DMP property for linear and nonlinear problems. Their derivation exploits the aforementioned relationships between flux and slope limiting. Next, we discuss the vertex-based version [30] of the Barth-Jespersen slope limiter [2] for general conservation laws and propose a more accurate slope limiting procedure. Using local bounds defined in terms of low-order reconstructions, we constrain the directional derivatives either via direct adjustment of their magnitudes or via the use of penalization terms in the discretized weak form of the governing equation. The aspects of entropy stabilization for nonlinear problems are briefly discussed in Section 5. The results of 2D numerical experiments in Section 6 illustrate the typical behavior of the presented limiting techniques in challenging situations (anisotropic layers, propagating fronts, steady-state conditions, nonlinear nonconvex flux functions). A grid convergence study is performed for a test problem with a smooth exact solution. In Section 7, we conclude with an outlook of how the presented limiting tools can be extended to systems and higher order space-time discretizations.

2. General limiting framework

Let $u(\mathbf{x}, t)$ be a scalar conserved quantity depending on the space location $\mathbf{x} \in \mathbb{R}^d$, $d \in \{1, 2, 3\}$ and time moment $t \geq 0$. We consider the generic scalar conservation law

$$\frac{\partial u}{\partial t} + \nabla \cdot \mathbf{f}(u) = 0, \quad (1)$$

where $\mathbf{f} = (f_1, \dots, f_d)$ is a (possibly nonlinear) flux function. Let K_i , $i \in \{1, \dots, E_h\}$ be a cell of a simplex or tensor product mesh. The union $\bar{\Omega}_h = \bigcup_{i=1}^{E_h} K_i$ of all mesh cells is the closure of a bounded computational domain. The boundary ∂K_i of the cell K_i consists of *faces* S_{ij} on which the unit outward normal \mathbf{n}_{ij} is constant. If $S_{ij} = \partial K_i \cap \partial K_j$ is a common boundary of two cells, then $j \in \{1, \dots, E_h\}$ is the index of the adjacent cell. Boundary faces $S_{ij} \subset \partial \Omega_h$ are numbered using indices $j \in \{E_h + 1, \dots, \bar{E}_h\}$. The indices of faces that form the boundary of K_i are stored in the set \mathcal{N}_i .

The DG- \mathbb{P}_1 method approximates $u \in L^2(\Omega_h)$ by a possibly discontinuous piecewise-linear function $u_h \in L^2(\Omega_h)$ such that $u_{ih} := u_h|_{K_i} \in \mathbb{P}_1(K_i)$ for $i = 1, \dots, E_h$. The normal flux $\mathbf{f}(u) \cdot \mathbf{n}_{ij}$ is approximated by a numerical flux $H(u_{ih}, u_{jh}, \mathbf{n}_{ij})$. If S_{ij} , $j > E_h$ is a face on the boundary $\partial \Omega_h$, then $u_{jh} = u_{ih}$ on $\{\mathbf{x} \in S_{ij} : \mathbf{f}'(u(\mathbf{x})) \cdot \mathbf{n}_{ij} \geq 0\}$. For $\mathbf{f}'(u_{ih}(\mathbf{x}, t)) \cdot \mathbf{n}_{ij} < 0$, the value of u_{jh} on S_{ij} is determined by an inflow boundary condition. The DG- \mathbb{P}_1 discretization of (1) on K_i is given by

$$\int_{K_i} w_{ih} \frac{\partial u_{ih}}{\partial t} d\mathbf{x} - \int_{K_i} \nabla w_{ih} \cdot \mathbf{f}(u_{ih}) d\mathbf{x} + \sum_{j \in \mathcal{N}_i} \int_{S_{ij}} w_{ih} H(u_{ih}, u_{jh}, \mathbf{n}_{ij}) ds = 0 \quad \forall w_{ih} \in \mathbb{P}_1(K_i). \quad (2)$$

Clearly, the accuracy and stability properties of such a method depend on the choice of the approximate Riemann solver $H(\cdot, \cdot, \cdot)$. In this work, we use the local Lax-Friedrichs (LLF) flux

$$H(u_L, u_R, \mathbf{n}_{ij}) = \mathbf{n}_{ij} \cdot \frac{\mathbf{f}(u_R) + \mathbf{f}(u_L)}{2} - \frac{1}{2} \lambda_{ij}(u_L, u_R)(u_R - u_L), \quad (3)$$

where λ_{ij} is the maximum wave speed of the 1D Riemann problem in the normal direction \mathbf{n}_{ij} , i.e.,

$$\lambda_{ij}(u_L, u_R) = \max_{\omega \in [0,1]} |\mathbf{f}'(\omega u_R + (1 - \omega)u_L) \cdot \mathbf{n}_{ij}|. \quad (4)$$

Using the test function $w_{ih} \equiv 1$, we find that the evolution of the cell average

$$U_{i0} = \frac{1}{|K_i|} \int_{K_i} u_{ih} d\mathbf{x} \quad (5)$$

is governed by the semi-discrete integral conservation law (cf. [31, 33])

$$|K_i| \frac{dU_{i0}}{dt} + \sum_{j \in \mathcal{N}_i} |S_{ij}| H_{ij}^{\mathbb{P}_1} = 0, \quad H_{ij}^{\mathbb{P}_1} = \frac{1}{|S_{ij}|} \int_{S_{ij}} H(u_{ih}, u_{jh}, \mathbf{n}_{ij}) ds. \quad (6)$$

The cell-centered finite volume (DG- \mathbb{P}_0) version of the LLF method is defined by

$$|K_i| \frac{dU_{i0}}{dt} + \sum_{j \in \mathcal{N}_i} |S_{ij}| H_{ij}^{\mathbb{P}_0} = 0, \quad H_{ij}^{\mathbb{P}_0} = H(U_{i0}, U_{j0}, \mathbf{n}_{ij}). \quad (7)$$

This piecewise-constant space discretization preserves all essential properties of the exact weak solution. If the system of ordinary differential equations (7) is discretized in time using a strong stability

preserving (SSP) Runge-Kutta method [14], the resulting fully discrete scheme is (locally) bound-preserving and satisfies a cell entropy inequality. These well-known properties of the LLF- \mathbb{P}_0 method can be easily verified using the theoretical framework developed by Guermond and Popov [17].

Unfortunately, the property-preserving LLF- \mathbb{P}_0 approximation is first-order accurate at best. The DG- \mathbb{P}_1 version (2) is up to second-order accurate but may converge to wrong weak solutions and/or violate discrete maximum principles. To cure this unsatisfactory behavior, we replace (2) with

$$\begin{aligned} \int_{K_i} w_{ih} \frac{\partial u_{ih}}{\partial t} d\mathbf{x} - \int_{K_i} \nabla w_{ih} \cdot \mathbf{f}(u_{ih}) d\mathbf{x} \\ + \sum_{j \in \mathcal{N}_i} \int_{S_{ij}} w_{ih} [\alpha_{ij} H(u_{ih}^*, u_{jh}^*, \mathbf{n}_{ij}) + (1 - \alpha_{ij}) H_{ij}^{\mathbb{P}_0}] ds = 0 \quad \forall w_{ih} \in \mathbb{P}_1(K_i), \end{aligned} \quad (8)$$

where $\alpha_{ij} \in [0, 1]$ is an adjustable flux correction factor such that $\alpha_{ji} = \alpha_{ij}$ and

$$u_{ih}^*(\underbrace{x_1, \dots, x_d}_{\mathbf{x}}, t) = U_{i0}(t) + \sum_{k=1}^d \beta_{ik} U_{ik}(t) (x_k - \bar{x}_{ik}) \quad (9)$$

is a limited Taylor expansion about the centroid $\bar{\mathbf{x}}_i = \frac{1}{|K_i|} \int_{K_i} \mathbf{x} d\mathbf{x}$. The multiplication of

$$U_{ik} := \frac{\partial u_{ih}}{\partial x_k}, \quad k = 1, \dots, d \quad (10)$$

by yet unspecified slope correction factors $\beta_{ik} \in [0, 1]$ makes it possible to adjust the magnitude of each partial derivative if necessary. On a non-periodic inflow boundary of Ω_h , we use the external limit $u_{jh}^* = u_{jh}$ since the value of u_{jh} , $j > E_h$ is defined by a Dirichlet boundary condition.

The semi-discrete evolution equation (8) corresponding to $w_{ih} \equiv 1$ blends (6) and (7) as follows:

$$|K_i| \frac{dU_{i0}}{dt} + \sum_{j \in \mathcal{N}_i} |S_{ij}| H_{ij}^* = 0, \quad (11)$$

$$H_{ij}^* = \frac{1}{|S_{ij}|} \int_{S_{ij}} [\alpha_{ij} H(u_{ih}^*, u_{jh}^*, \mathbf{n}_{ij}) + (1 - \alpha_{ij}) H_{ij}^{\mathbb{P}_0}] ds. \quad (12)$$

Note that the limited flux H_{ij}^* reduces to $H_{ij}^{\mathbb{P}_1}$ for $\alpha_{ij} = \beta_{ik} = \beta_{jk} = 1$, $k = 1, \dots, d$. The flux $H_{ij}^{\mathbb{P}_0}$ is recovered if we set $\alpha_{ij} = 0$ or $\beta_{ik} = \beta_{jk} = 0$, $k = 1, \dots, d$. Hence, the desired properties of the low-order LLF scheme (7) can always be preserved by tuning α_{ij} and/or (β_{ik}, β_{jk}) .

Let us discretize (8) in time using an explicit SSP Runge-Kutta method [14] such that each stage has the structure of a forward Euler update. The fully discrete counterpart of (11) is given by

$$U_{i0}^* = U_{i0} - \frac{\Delta t}{|K_i|} \sum_{j \in \mathcal{N}_i} |S_{ij}| H_{ij}^*, \quad (13)$$

where $\Delta t > 0$ is the time step. The flux H_{ij}^* is calculated using the data from the previous time level or SSP-RK stage. We constrain U_{i0}^* to satisfy a (local) discrete maximum principle of the form

$$U_{i0}^{\min} \leq U_{i0}^* \leq U_{i0}^{\max}. \quad (14)$$

The choice of the bounds U_{i0}^{\min} and U_{i0}^{\max} must guarantee that the DMP constraints (14) hold at least in the case of $H_{ij}^* = H_{ij}^{\mathbb{P}_0}$ for all $j \in \mathcal{N}_i$. We will define such *feasible* bounds in Section 3.

Substituting U_{i0}^* defined by (13) into (14), we obtain the equivalent inequality constraints

$$\frac{|K_i|}{\Delta t}(U_{i0}^{\min} - U_{i0}) \leq - \sum_{j \in \mathcal{N}_i} |S_{ij}| H_{ij}^* \leq \frac{|K_i|}{\Delta t}(U_{i0}^{\max} - U_{i0}), \quad (15)$$

the validity of which can be enforced via direct flux limiting (adjustment of α_{ij} , as discussed in Section 3) and/or slope limiting (adjustment of β_{ik}, β_{jk} , as discussed in Section 4). The latter approach is commonly preferred in DG methods (cf. [12, 24, 30]). However, instead of constraining the linear polynomials u_{ih}^* defined by (9) in a way which guarantees that conditions (15) are satisfied for H_{ij}^* defined by (12), many slope limiters impose linear inequality constraints of the form

$$U_{ip}^{\min} \leq u_{ih}^*(\mathbf{x}_{ip}) \leq U_{ip}^{\max} \quad (16)$$

on the values of u_{ih}^* at certain control points \mathbf{x}_{ip} . In many cases, these constraints are not equivalent to (15). If they are more restrictive, the slope limiter may fail to recognize a well-resolved gradient. If the bounds are too wide, the resulting cell averages U_{ih}^* may violate (14).

In this work, we develop both slope limiters which guarantee the validity of DMP constraints and DG- \mathbb{P}_1 methods based on the following design principles for flux and slope limiting:

- cell averages U_{ih}^* must be kept in bounds using a flux limiter ($\alpha_{ij} \in [0, 1]$) to enforce (15);
- linear polynomials u_{ih}^* may be constrained using a slope limiter based on inequality constraints for pointwise values $u_{ih}^*(\mathbf{x}_{ip})$ or partial derivatives $U_{ik}^* = \frac{\partial u_{ih}^*}{\partial x_k} = \beta_{ik} \frac{\partial u_{ih}}{\partial x_k}$, $k = 1, \dots, d$.

According to this design philosophy, the purpose of slope limiting is not to produce a flux H_{ij}^* satisfying conditions (15) but to prevent unbounded growth of the partial derivatives U_{ik}^* . Failure to do so would result in an inaccurate approximation to the cell averages U_{i0}^* which represent the primary unknowns of our method. Similarly to reconstruction-based finite volume and DG methods, the additional Taylor degrees of freedom U_{ik}^* are needed just to compute fluxes H_{ij}^* that are more accurate than $H_{ij}^{\mathbb{P}_0}$.

3. Flux limiting

Let us begin with the presentation and analysis of flux limiters, i.e., algorithms for calculating correction factors $\alpha_{ij} \in [0, 1]$ such that the symmetry condition $\alpha_{ij} = \alpha_{ji}$ holds and

- H_{ij}^* defined by (12) satisfies (15) for a given pair of slope-limited traces $u_{ih}^*|_{S_{ij}}$ and $u_{jh}^*|_{S_{ij}}$;

- $H_{ji}^* = -H_{ij}^*$ satisfies similar DMP constraints for the cell average U_{j0}^* if $1 \leq j \leq E_h$.

Additionally, a well-designed flux limiter should produce $\alpha_{ij} = 1$ in regions where this setting does not drive the cell averages of the DG- \mathbb{P}_1 solution out of bounds.

The hybrid LLF flux (12) can be written as $H_{ij}^* = H_{ij}^{\mathbb{P}_0} - \frac{F_{ij}^*}{|S_{ij}|}$, where $H_{ij}^{\mathbb{P}_0}$ is defined by (7) and

$$F_{ij}^* = \alpha_{ij} F_{ij}, \quad F_{ij} = |S_{ij}|(H_{ij}^{\mathbb{P}_0} - H_{ij}^{\mathbb{P}_1}). \quad (17)$$

Using this representation of H_{ij}^* in terms of the low-order components $H_{ij}^{\mathbb{P}_0}$ and limited counterparts F_{ij}^* of the antidiffusive fluxes F_{ij} , the DMP constraints (15) can be written as

$$\frac{|K_i|}{\Delta t}(U_{i0}^{\min} - U_{i0}^{\mathbb{P}_0}) \leq \sum_{j \in \mathcal{N}_i} F_{ij}^* \leq \frac{|K_i|}{\Delta t}(U_{i0}^{\max} - U_{i0}^{\mathbb{P}_0}), \quad (18)$$

where

$$U_{i0}^{\mathbb{P}_0} = U_{i0} - \frac{\Delta t}{|K_i|} \sum_{j \in \mathcal{N}_i} |S_{ij}| H_{ij}^{\mathbb{P}_0}. \quad (19)$$

The result of flux correction depends on the choice of the bounds and on the practical algorithm for calculating correction factors $\alpha_{ij} \in [0, 1]$ that guarantee the validity of (18) under certain time step restrictions. We elaborate on these choices and analyze two simple flux limiters below.

3.1. Bounds for DMP constraints

For (18) to be satisfied at least for the trivial choice $\alpha_{ij} = 0 \ \forall j \in \mathcal{N}_i$, the bounds U_{i0}^{\min} and U_{i0}^{\max} should be admissible in the sense that $U_{i0}^{\min} \leq U_{i0}^{\mathbb{P}_0} \leq U_{i0}^{\max}$. In particular, this will be the case if $U_{i0}^{\min} = u^{\min}$ and $U_{i0}^{\max} = u^{\max}$ are some global bounds such that $U_{i0}^{\mathbb{P}_0} \in [u^{\min}, u^{\max}]$. The use of global bounds may be appropriate, e.g., if the slope-limited linear polynomials u_{ih}^* and u_{jh}^* are constrained to satisfy local maximum principles at certain points on S_{ij} (see [11] and Section 4.2 below). In this case, the target fluxes $H_{ij} = H_{ij}^{\mathbb{P}_0} - \frac{F_{ij}}{|S_{ij}|}$ produce essentially nonoscillatory approximations and it is sufficient to enforce the validity of a global DMP for cell averages. For example, a flux limiter based on (18) with global bounds $U_{i0}^{\min} = 0$ and $U_{i0}^{\max} = 1$ may be used to keep cell-averaged concentrations in the range $[0, 1]$ if the slope limiting procedure does not guarantee this property.

In many cases, however, a better limiting strategy is to enforce local DMPs at the flux limiting stage. Then slope limiting can be performed in a safe mode under less restrictive constraints, as formulated in Section 4.3. Adopting this design philosophy, we define local bounds

$$U_{i0}^{\max} = \max_{j \in \mathcal{J}_{i0}} U_{j0}, \quad U_{i0}^{\min} = \min_{j \in \mathcal{J}_{i0}} U_{j0}, \quad (20)$$

where \mathcal{J}_{i0} is a *bounding stencil* containing i and (a subset of) indices of cells K_j that share a common vertex with K_i . By default, the indices of all common-vertex neighbors are included in \mathcal{J}_{i0} but better monotonicity preservation for anisotropic transport in layers can be achieved by including only neighbors belonging to the same layer in the definition of \mathcal{J}_{i0} . The first numerical example of Section 6 demonstrates the potential benefits of using such anisotropic local bounds for U_{i0}^* .

3.2. Localized FCT limiting

After choosing the bounds, a set of correction factors α_{ij} satisfying conditions (18) and other flux limiting criteria needs to be found. Introducing the bounding fluxes

$$F_{ij}^{\max} = \begin{cases} \frac{|K_i|}{\Delta t} \frac{|S_{ij}|}{|\partial K_i|} \max\{0, \min\{U_{i0}^{\max} - U_{i0}^{\mathbb{P}_0}, U_{j0}^{\mathbb{P}_0} - U_{j0}^{\min}\}\} & \text{if } 1 \leq j \leq E_h, \\ \frac{|K_i|}{\Delta t} \frac{|S_{ij}|}{|\partial K_i|} \max\{0, U_{i0}^{\max} - U_{i0}^{\mathbb{P}_0}\} & \text{otherwise,} \end{cases} \quad (21)$$

$$F_{ij}^{\min} = \begin{cases} \frac{|K_i|}{\Delta t} \frac{|S_{ij}|}{|\partial K_i|} \min\{0, \max\{U_{i0}^{\min} - U_{i0}^{\mathbb{P}_0}, U_{j0}^{\mathbb{P}_0} - U_{j0}^{\max}\}\} & \text{if } 1 \leq j \leq E_h, \\ \frac{|K_i|}{\Delta t} \frac{|S_{ij}|}{|\partial K_i|} \min\{0, U_{i0}^{\min} - U_{i0}^{\mathbb{P}_0}\} & \text{otherwise,} \end{cases} \quad (22)$$

a localized version [10, 42] of Zalesak's [46] flux-corrected transport (FCT) algorithm defines

$$\alpha_{ij} = \begin{cases} \min\left\{1, \frac{F_{ij}^{\max}}{F_{ij}}\right\} & \text{if } F_{ij} > 0, \\ 1 & \text{if } F_{ij} = 0, \\ \min\left\{1, \frac{F_{ij}^{\min}}{F_{ij}}\right\} & \text{if } F_{ij} < 0. \end{cases} \quad (23)$$

Recall that S_{ij} is an interior face for $1 \leq j \leq E_h$ and a face on the boundary $\partial\Omega_h$ for $E_h + 1 \leq j \leq \bar{E}_h$.

3.3. Monolithic convex limiting

The monolithic convex limiting (MCL) procedure [31, 32, 34, 33] replaces (21) and (22) with

$$F_{ij}^{\max} = \begin{cases} \lambda_{ij}^{\mathbb{P}_0} |S_{ij}| \max\{0, \min\{U_{i0}^{\max} - \bar{U}_{ij,0}, \bar{U}_{ji,0} - U_{j0}^{\min}\}\} & \text{if } 1 \leq j \leq E_h, \\ \lambda_{ij}^{\mathbb{P}_0} |S_{ij}| \max\{0, U_{i0}^{\max} - \bar{U}_{ij,0}\} & \text{otherwise,} \end{cases} \quad (24)$$

$$F_{ij}^{\min} = \begin{cases} \lambda_{ij}^{\mathbb{P}_0} |S_{ij}| \min\{0, \max\{U_{i0}^{\min} - \bar{U}_{ij,0}, \bar{U}_{ji,0} - U_{j0}^{\max}\}\} & \text{if } 1 \leq j \leq E_h, \\ \lambda_{ij}^{\mathbb{P}_0} |S_{ij}| \min\{0, U_{i0}^{\min} - \bar{U}_{ij,0}\} & \text{otherwise,} \end{cases} \quad (25)$$

where $\lambda_{ij}^{\mathbb{P}_0} = \lambda_{ij}(U_{i0}, U_{j0})$ is the maximum wave speed (4) of the LLF- \mathbb{P}_0 approximation (7) and

$$\bar{U}_{ij,0} = \frac{U_{j0} + U_{i0}}{2} - \mathbf{n}_{ij} \cdot \frac{\mathbf{f}(U_{j0}) - \mathbf{f}(U_{i0})}{2\lambda_{ij}^{\mathbb{P}_0}} \quad (26)$$

are the *bar states* (as originally defined in [18]) of the property-preserving LLF- \mathbb{P}_0 approximation.

Using the mean value theorem of calculus, it is easy to show that the states $\bar{U}_{ij,0}$ satisfy [32]

$$\min\{U_{i0}, U_{j0}\} \leq \bar{U}_{ij,0} \leq \max\{U_{i0}, U_{j0}\}. \quad (27)$$

These estimates will also hold if λ_{ij} defined by (4) is replaced with an arbitrary upper bound $\lambda_{ij}^{\max} \geq \lambda_{ij}$.

The DMP properties of FCT and MCL flux limiters are summarized in the following theorem which adapts the analysis presented in [31, 32, 33] to the setting of this paper for the reader's convenience.

Theorem 1 (DMP property of FCT and MCL flux limiters). *Define the correction factors α_{ij} using formula (23) with flux bounds (21),(22) or (24),(25) corresponding to*

$$U_{i0}^{\max} \geq \max_{j \in \mathcal{N}_i} U_{j0}, \quad U_{i0}^{\min} \leq \min_{j \in \mathcal{N}_i} U_{j0}. \quad (28)$$

Choose a time step Δt satisfying the CFL-like condition

$$\frac{\Delta t}{|K_i|} \sum_{j \in \mathcal{N}_i} |S_{ij}| \lambda_{ij} \leq 1. \quad (29)$$

Then update (13) with limited fluxes H_{ij}^ defined by (12) satisfies the DMP constraints (14) in the case of periodic boundary conditions.*

PROOF. The SSP Runge-Kutta stage (13) admits the following equivalent representations (cf. [18, 32])

$$U_{i0}^* = U_{i0} + \frac{\Delta t}{|K_i|} \sum_{j \in \mathcal{N}_i} (|S_{ij}| \lambda_{ij} (\bar{U}_{ij,0} - U_{i0}) + F_{ij}^*) \quad (30)$$

$$= U_{i0}^{\mathbb{P}_0} + \frac{\Delta t}{|K_i|} \sum_{j \in \mathcal{N}_i} F_{ij}^* \quad (31)$$

$$= U_{i0} + \frac{\Delta t}{|K_i|} \sum_{j \in \mathcal{N}_i} |S_{ij}| \lambda_{ij} (\bar{U}_{ij,0}^* - U_{i0}), \quad (32)$$

where $U_{i0}^{\mathbb{P}_0} = U_{i0} + \frac{\Delta t}{|K_i|} \sum_{j \in \mathcal{N}_i} |S_{ij}| \lambda_{ij} (\bar{U}_{ij,0} - U_{i0})$ is the result of a forward Euler step for (7) and

$$\bar{U}_{ij,0}^* = \bar{U}_{ij,0} + \frac{F_{ij}^*}{|S_{ij}| \lambda_{ij}} = \bar{U}_{ij,0} + \frac{\alpha_{ij} F_{ij}}{|S_{ij}| \lambda_{ij}}. \quad (33)$$

are flux-corrected counterparts of the \mathbb{P}_0 bar states $\bar{U}_{ij,0}$ defined by (26). Invoking (27) and (28), we find that $\bar{U}_{ij,0} \in [U_{i0}^{\min}, U_{i0}^{\max}]$. If the time step Δt satisfies (29) then

$$U_{i0}^* = \left(1 - \frac{\Delta t}{|K_i|} \sum_{j \in \mathcal{N}_i} |S_{ij}| \lambda_{ij} \right) U_{i0} + \frac{\Delta t}{|K_i|} \sum_{j \in \mathcal{N}_i} |S_{ij}| \lambda_{ij} \bar{U}_{ij,0}^* \quad (34)$$

is a convex combination of U_{i0} and $\bar{U}_{ij,0}^*$. Therefore, update (34) is bound-preserving if the choice of α_{ij} in (33) guarantees that $U_{ij,0}^* \in [U_{i0}^{\min}, U_{i0}^{\max}]$ for $j \in \mathcal{N}_i$. In particular, this sufficient condition is satisfied for the trivial choice $\alpha_{ij} = 0$. It follows that $U_{i0}^{\mathbb{P}_0} \in [U_{i0}^{\min}, U_{i0}^{\max}]$.

If α_{ij} are defined by (23) with the MCL bounds (24),(25) then the BP property of $U_{ij,0}^*$ follows from the estimates $F_{ij}^{\min} \leq \alpha_{ij} F_{ij} \leq F_{ij}^{\max}$ by definition of F_{ij}^{\min} and F_{ij}^{\max} , as originally shown in [32]. For α_{ij} defined by (23) with the FCT bounds (21),(22), the limited fluxes satisfy

$$\frac{|K_i|}{\Delta t} \frac{|S_{ij}|}{|\partial K_i|} (U_{i0}^{\min} - U_{i0}^{\mathbb{P}_0}) \leq F_{ij}^* = \alpha_{ij} F_{ij} \leq \frac{|K_i|}{\Delta t} \frac{|S_{ij}|}{|\partial K_i|} (U_{i0}^{\max} - U_{i0}^{\mathbb{P}_0}) \quad (35)$$

with $\alpha_{ij} \in [0, 1]$ provided that $U_{i0}^{\mathbb{P}_0} \in [U_{i0}^{\min}, U_{i0}^{\max}]$. As shown above, the low-order LLF approximation $U_{i0}^{\mathbb{P}_0}$ is in bounds for time steps satisfying (29). Substituting estimates (35) into (31), we find that the assertion of the theorem is true for the localized FCT limiter as well. \square

Remark 1. Condition (28) may be violated if \mathcal{N}_i is not a subset of the set \mathcal{J}_{i0} that we used to define the local bounds in (20), i.e., if not all common face neighbors are included to use the option of anisotropic flux limiting. In this case, our definitions (21),(22) and (24),(25) of the bounding fluxes automatically extend the bounds to include the admissible states $U_{i0}^{\mathbb{P}_0}$ and $\bar{U}_{ij,0}$, respectively.

Remark 2. A linear flux function $\mathbf{v}u$ depending on a spatially variable velocity field $\mathbf{v} = \mathbf{v}(\mathbf{x})$ is not of the form $\mathbf{f}(u)$. As shown in [33], definition (26) of the bar states $\bar{U}_{ij,0}$ should be replaced with

$$\bar{U}_{ij,0} = \frac{U_{j0} + U_{i0}}{2} - \left(\frac{\int_{S_{ij}} \mathbf{v} \cdot \mathbf{n}_{ij} \, ds}{\int_{S_{ij}} |\mathbf{v} \cdot \mathbf{n}_{ij}| \, ds} \right) \frac{U_{j0} - U_{i0}}{2}$$

in the case of the linear advection equation. Moreover, the additional ‘reactive’ term

$$-\frac{\Delta t}{|K_i|} U_{i0} \sum_{j \in \mathcal{N}_i} \int_{S_{ij}} \mathbf{v} \cdot \mathbf{n}_{ij} \, ds$$

appears on the right-hand sides of (30)–(32). If the vector field \mathbf{v} is not divergence-free, only positivity preservation can be guaranteed for the exact and numerical solution.

A detailed description of FCT and MCL flux limiters for the linear advection equation (including DMP analysis for non-periodic boundary conditions) can be found in [33], where such limiters were used to constrain the cell averages of a $\mathbb{P}_1 \oplus \mathbb{P}_0$ enriched Galerkin approximation. The two limiting approaches produce very similar results for time-dependent hyperbolic problems but the MCL version is better suited for calculating stationary solutions because the flux bounds (24),(25) are independent of the (pseudo-)time step Δt , and so is the fixed point solution to which (13) converges. For that reason, we perform flux limiting using the MCL version of (23) in the numerical experiments of Section 6.

4. Slope limiting

The traditional purpose of slope limiting in DG methods is to enforce inequality constraints for pointwise values of numerical solutions *assuming* that the cell averages are bound-preserving. This assumption is generally not true but slope limiting preconstraints the numerical fluxes in a way which makes violations of (14) less likely or even provably impossible. In this section, we discuss three ways to construct slope limiters. The first approach guarantees the validity of (15). The limiting formula for the linear advection equation is relatively simple and equivalent to (23) in the 1D case. The one for nonlinear problems is derived using linear sufficient conditions. The second slope limiter ensures that the value of the linear polynomial u_{ih}^* at each vertex of K_i is bounded by the maximum and minimum of U_{j0} in cells K_j containing the vertex [30]. This limiter is generally not BP but produces nonoscillatory

solutions even in the absence of flux limiting. The third approach that we consider is slope limiting based on inequality constraints for the partial derivatives $U_{ik}^* = \frac{\partial u_{ih}^*}{\partial x_k}$ rather than pointwise values of u_{ih}^* . Delegating enforcement of the DMP constraints (14) to the flux limiters presented in Section 3, this algorithm keeps U_{ik}^* , $k = 1, \dots, d$ in bounds that depend on low-order reconstructions from cell averages. The first two limiters are *isotropic*, i.e., they use $\beta_{i1} = \dots = \beta_{id} = \beta_i \in [0, 1]$ in (9). The third slope limiter is *anisotropic* in the sense that individually chosen correction factors β_{ik} are applied to U_{ik} , $k = 1, \dots, d$. A monolithic version of this limiter penalizes violations of the inequality constraints for U_{ik}^* without manipulating the partial derivatives U_{ik} of the DG- \mathbb{P}_1 solution directly.

4.1. Isotropic slope limiting under flux constraints

We begin with the derivation of a slope limiter based on the flux constraints (15) for a linear conservation law. If the flux limiter is deactivated by setting $\alpha_{ij} = 1 \ \forall j \in \mathcal{N}_i$, and an isotropic slope limiting strategy is adopted, the limited flux H_{ij}^* , $1 \leq j \leq E_h$ defined by (9) and (12) reduces to

$$H_{ij}^* = \frac{1}{|S_{ij}|} \int_{S_{ij}} H(U_{i0} + \beta_i(u_{ih} - U_{i0}), U_{j0} + \beta_j(u_{jh} - U_{j0}), \mathbf{n}_{ij}) \, ds, \quad (36)$$

where $u_{ih} \in \mathbb{P}_1(K_i)$ is the unconstrained DG- \mathbb{P}_1 solution, U_{i0} is its average in K_i and $\beta_i \in [0, 1]$ is the isotropic slope limiting factor for the constant gradient of u_{ih} .

In the case of a linear advection equation with $\mathbf{f}(u) = \mathbf{v}u$, the LLF flux becomes the upwind flux

$$H(u_L, u_R, \mathbf{n}) = \begin{cases} (\mathbf{v} \cdot \mathbf{n})u_R & \text{if } \mathbf{v} \cdot \mathbf{n} < 0, \\ 0 & \text{if } \mathbf{v} \cdot \mathbf{n} = 0, \\ (\mathbf{v} \cdot \mathbf{n})u_L & \text{if } \mathbf{v} \cdot \mathbf{n} > 0 \end{cases} \quad (37)$$

and, therefore, the corresponding limited flux H_{ij}^* can be written as

$$H_{ij}^* = H_{ij}^{\mathbb{P}_0} + \frac{\beta_i}{|S_{ij}|} \int_{S_{ij} \cap \partial K_+} (u_{ih} - U_{i0}) \mathbf{v} \cdot \mathbf{n}_{ij} \, ds + \frac{\beta_j}{|S_{ij}|} \int_{S_{ij} \cap \partial K_-} (u_{jh} - U_{j0}) \mathbf{v} \cdot \mathbf{n}_{ij} \, ds, \quad (38)$$

where $\partial K_+ = \{\mathbf{x} \in \partial K : \mathbf{v} \cdot \mathbf{n} > 0\}$ and $\partial K_- = \{\mathbf{x} \in \partial K : \mathbf{v} \cdot \mathbf{n} < 0\}$ are the outlet and inlet of ∂K_i .

It follows that the validity of the inequality constraints (18) for $F_{ij}^* := F_{ij}$, where

$$F_{ij} = \beta_i \int_{S_{ij} \cap \partial K_+} (U_{i0} - u_{ih}) \mathbf{v} \cdot \mathbf{n}_{ij} \, ds + \beta_j \int_{S_{ij} \cap \partial K_-} (U_{j0} - u_{jh}) \mathbf{v} \cdot \mathbf{n}_{ij} \, ds \quad (39)$$

can be enforced by using the slope correction factors

$$\beta_i = \min_{j \in \mathcal{N}_i^+} \begin{cases} \alpha_{ij}^+ & \text{if } \int_{S_{ij} \cap \partial K_+} (U_{i0} - u_{ih}) \mathbf{v} \cdot \mathbf{n}_{ij} \, ds > 0, \\ 1 & \text{if } \int_{S_{ij} \cap \partial K_+} (U_{i0} - u_{ih}) \mathbf{v} \cdot \mathbf{n}_{ij} \, ds = 0, \\ \alpha_{ij}^- & \text{if } \int_{S_{ij} \cap \partial K_+} (U_{i0} - u_{ih}) \mathbf{v} \cdot \mathbf{n}_{ij} \, ds < 0, \end{cases} \quad (40)$$

where \mathcal{N}_i^+ is the set of faces S_{ij} such that $|S_{ij} \cap \partial K_+| > 0$ for $\partial K_+ = \{\mathbf{x} \in \partial K : \mathbf{v} \cdot \mathbf{n} > 0\}$ and

$$\alpha_{ij}^+ = \min \left\{ 1, \frac{F_{ij}^{\max}}{F_{ij}^+} \right\}, \quad \alpha_{ij}^- = \min \left\{ 1, \frac{F_{ij}^{\min}}{F_{ij}^-} \right\} \quad (41)$$

are the face-based correction factors that formula (23) would produce for the antidiffusive fluxes

$$F_{ij}^+ = \max \left\{ 0, \int_{S_{ij} \cap \partial K_+} (U_{i0} - u_{ih}) \mathbf{v} \cdot \mathbf{n}_{ij} \, ds \right\} + \max \left\{ 0, \int_{S_{ij} \cap \partial K_-} (U_{j0} - u_{jh}) \mathbf{v} \cdot \mathbf{n}_{ij} \, ds \right\}, \quad (42)$$

$$F_{ij}^- = \min \left\{ 0, \int_{S_{ij} \cap \partial K_+} (U_{i0} - u_{ih}) \mathbf{v} \cdot \mathbf{n}_{ij} \, ds \right\} + \min \left\{ 0, \int_{S_{ij} \cap \partial K_-} (U_{j0} - u_{jh}) \mathbf{v} \cdot \mathbf{n}_{ij} \, ds \right\}. \quad (43)$$

The structure of this new isotropic slope limiter is similar to that of Zalesak's FCT flux limiter [46].

Remark 3. If $S_{ij} \subset \partial \Omega_h$, which is the case for $E_h + 1 \leq j \leq \bar{E}_h$, and a Dirichlet boundary data u_{jh} is prescribed at the inlet $S_{ij} \cap \partial K_- = \{\mathbf{x} \in S_{ij} : \mathbf{v} \cdot \mathbf{n} < 0\}$, then we have

$$F_{ij} = \beta_i \int_{S_{ij} \cap \partial K_+} (U_{i0} - u_{ih}) \mathbf{v} \cdot \mathbf{n}_{ij} \, ds \quad (44)$$

and the boundary integrals over $S_{ij} \cap \partial K_-$ should be omitted in definitions (42), (43).

Theorem 2 (DMP property of the new slope limiter with linear flux constraints). *Let slope limiting be performed using formula (40) under assumptions of Theorem 1. Then update (13) with H_{ij}^* defined by (38) satisfies the DMP constraints (14).*

PROOF. Using (39)–(43), we obtain the estimates $F_i^{\min} \leq \alpha_{ij}^- F_{ij}^- \leq F_{ij} \leq \alpha_{ij}^+ F_{ij}^+ \leq F_{ij}^{\max}$. The validity of the discrete maximum principle follows as in the proof of Theorem 1. \square

Remark 4. For the 1D linear advection equation $\frac{\partial u}{\partial t} + v \frac{\partial u}{\partial x} = 0$ with constant velocity $v \in \mathbb{R} \setminus \{0\}$, the set \mathcal{N}_i^+ consists of a single index j . In this case, formula (40) produces $\beta_i = \alpha_{ij}$, where α_{ij} is given by (23) with the upwind-sided antidiffusive flux $F_{ij} = |v|(U_{i0} - u_{ih}|_{S_{ij}}) = H_{ij}^{\mathbb{P}_0} - H_{ij}^{\mathbb{P}_1}$. Hence, the slope limiter defined by (40) is equivalent to the generic flux limiter defined by (23).

In the case of a nonlinear conservation law, the limited flux (36) depends on β_i and β_j in a nonlinear manner. However, linearized sandwich estimates of the form (cf. [41])

$$F_{ij}^{\min} \leq \alpha_{ij}^- F_{ij}^- \leq F_{ij}(\beta_i, \beta_j) \leq \alpha_{ij}^+ F_{ij}^+ \leq F_{ij}^{\max} \quad \forall \beta_i, \beta_j \leq \min\{\alpha_{ij}^+, \alpha_{ij}^-\} \quad (45)$$

with α_{ij}^\pm defined by (41) can be used to enforce (14) again. Introducing

$$P_{ij}^+ = \int_{S_{ij}} \max\{0, U_{i0} - u_{ih}\} \, ds, \quad P_{ij}^- = \int_{S_{ij}} \min\{0, U_{i0} - u_{ih}\} \, ds, \quad (46)$$

we define the correction factor β_i of the slope limiter with nonlinear flux constraints as follows:

$$\beta_i = \min_{j \in \mathcal{N}_i} \begin{cases} \min\{\alpha_{ij}^+, \alpha_{ij}^-\} & \text{if } P_{ij}^+ > 0, P_{ij}^- < 0, \\ \alpha_{ij}^+ & \text{if } P_{ij}^+ > 0, P_{ij}^- = 0, \\ \alpha_{ij}^- & \text{if } P_{ij}^+ = 0, P_{ij}^- < 0, \\ 1 & \text{if } P_{ij}^+ = 0, P_{ij}^- = 0. \end{cases} \quad (47)$$

To derive the bounding fluxes F_{ij}^\pm for (45), we need to estimate $F_{ij}(\beta_i, \beta_j)$. Let us define the general LLF flux (3) for (36) using an upper bound λ_{ij}^{\max} for the maximum wave speed such that

$$\lambda_{ij}^{\max} \geq \lambda_{ij}(U_{i0} + \beta_i(u_{ih} - U_{i0}), U_{j0} + \beta_j(u_{jh} - U_{j0})) \quad \forall \beta_i, \beta_j \in [0, 1]. \quad (48)$$

Then the slope-limited antidiffusive flux is given by $F_{ij}(\beta_i, \beta_j) = \int_{S_{ij}} G(\beta_i, \beta_j, \mathbf{n}_{ij}) \, ds$, where

$$\begin{aligned} G(\beta_i, \beta_j, \mathbf{n}_{ij}) &= \mathbf{n}_{ij} \cdot \frac{\mathbf{f}(U_{j0}) - \mathbf{f}(U_{j0} + \beta_j(u_{jh} - U_{j0}))}{2} \\ &\quad + \mathbf{n}_{ij} \cdot \frac{\mathbf{f}(U_{i0}) - \mathbf{f}(U_{i0} + \beta_i(u_{ih} - U_{i0}))}{2} \\ &\quad - \frac{\lambda_{ij}^{\max}}{2} [\beta_j(U_{j0} - u_{jh}) - \beta_i(U_{i0} - u_{ih})]. \end{aligned} \quad (49)$$

By the mean value theorem, there exist intermediate states u_R and u_L such that

$$\mathbf{n}_{ij} \cdot [\mathbf{f}(U_{j0}) - \mathbf{f}(U_{j0} + \beta_j(u_{jh} - U_{j0}))] = \beta_j \mathbf{n}_{ij} \cdot \mathbf{f}'(u_R)(u_{jh} - U_{j0}), \quad (50)$$

$$\mathbf{n}_{ij} \cdot [\mathbf{f}(U_{i0}) - \mathbf{f}(U_{i0} + \beta_i(u_{ih} - U_{i0}))] = \beta_i \mathbf{n}_{ij} \cdot \mathbf{f}'(u_L)(u_{ih} - U_{i0}), \quad (51)$$

where $|\mathbf{n}_{ij} \cdot \mathbf{f}'(u_R)| \leq \lambda_{ij}^{\max}$ and $|\mathbf{n}_{ij} \cdot \mathbf{f}'(u_L)| \leq \lambda_{ij}^{\max}$ by definition of λ_{ij}^{\max} as an upper bound for the maximum wave speed. It follows that conditions (45) are satisfied for the bounding fluxes

$$F_{ij}^+ = \lambda_{ij}^{\max} \int_{S_{ij}} (\max\{0, U_{i0} - u_{ih}\} - \min\{0, U_{j0} - u_{jh}\}) \, ds = \lambda_{ij}^{\max} (P_{ij}^+ - P_{ji}^-), \quad (52)$$

$$F_{ij}^- = \lambda_{ij}^{\max} \int_{S_{ij}} (\min\{0, U_{i0} - u_{ih}\} - \max\{0, U_{j0} - u_{jh}\}) \, ds = \lambda_{ij}^{\max} (P_{ij}^- - P_{ji}^+). \quad (53)$$

Theorem 3 (DMP property of the new slope limiter with nonlinear flux constraints). *Let slope limiting be performed using formula (47) under assumptions of Theorem 1. Then update (13) with H_{ij}^* defined by (12) satisfies the DMP constraints (14) for any choice of $\alpha_{ij} \in [0, 1]$.*

PROOF. The proof is similar to that of Theorem 2. \square

Remark 5. In principle, the nonlinear flux constraints $F_{ij}^{\min} \leq F_{ij}(\beta_i, \beta_j) \leq F_{ij}^{\max}$ can be enforced using optimization-based methods to determine the values of β_i and β_j . However, the high cost of solving nonlinear inequality-constrained optimization problems makes this approach impractical since the same DMP constraints can be easily enforced using the flux limiters presented in Section 3.

In summary, slope limiting under flux constraints can guarantee the DMP property of cell averages in the nonlinear case as well. Unfortunately, the resulting schemes are either costly or based on pessimistic estimates. The slope limiters to be presented next are based on linear inequality constraints. These limiters do not control the cell averages directly but provide sufficiently accurate input for subsequent flux limiting, which is our preferred approach to keeping the cell averages in bounds.

4.2. Isotropic slope limiting under solution constraints

Instead of enforcing the flux constraints (15), the slopes of the DG solution can be adjusted to ensure that the value of the linear polynomial $u_{ih}^* = U_{i0} + \beta_i(u_{ih} - U_{i0})$ at any point $\mathbf{x} \in K_i$ will be bounded by the maximum and minimum of cell averages in surrounding cells [30]. Since u_{ih}^* attains its extrema at the vertices $\mathbf{x}_{i1}, \dots, \mathbf{x}_{iN}$ of K_i , it is sufficient to ensure that the pointwise values $u_{ih}(\mathbf{x}_{ip})$, $p = 1, \dots, N$ are in bounds. The vertex-based DG version [30] of the Barth-Jespersen slope limiter [2] for finite volume schemes is designed to enforce inequality constraints of the form

$$U_{ip}^{\min} \leq u_{ih}^*(\mathbf{x}_{ip}) = U_{i0} + \beta_i(u_{ih}(\mathbf{x}_{ip}) - U_{i0}) \leq U_{ip}^{\max}, \quad p = 1, \dots, N \quad (54)$$

using the correction factor

$$\beta_i = \min_{1 \leq p \leq N} \begin{cases} \min \left\{ 1, \frac{U_{ip}^{\max} - U_{i0}}{u_{ih}(\mathbf{x}_{ip}) - U_{i0}} \right\} & \text{if } u_{ih}(\mathbf{x}_{ip}) > U_{i0}, \\ 1 & \text{if } u_{ih}(\mathbf{x}_{ip}) = U_{i0}, \\ \min \left\{ 1, \frac{U_{ip}^{\min} - U_{i0}}{u_{ih}(\mathbf{x}_{ip}) - U_{i0}} \right\} & \text{if } u_{ih}(\mathbf{x}_{ip}) < U_{i0}. \end{cases} \quad (55)$$

Remarkably, this formula has the same structure as definition (23) of the flux correction factors α_{ij} .

By default, the local bounds U_{ip}^{\min} and U_{ip}^{\max} of the vertex-based (VB) slope limiter are defined by

$$U_{ip}^{\max} = \max_{j \in \mathcal{E}_{ip}} U_{j0}, \quad U_{ip}^{\min} = \min_{j \in \mathcal{E}_{ip}} U_{j0}, \quad (56)$$

where \mathcal{E}_{ip} is the integer set containing the indices of cells that meet at the vertex \mathbf{x}_{ip} , $p \in \{1, \dots, N\}$.

As demonstrated, e.g., in [4], the isotropic VB slope limiter defined by (54) and (55) belongs to the most accurate limiting techniques for DG schemes. It is easy to implement and typically produces solutions that are free of undershoots and overshoots. However, it is not provably bound-preserving if no flux limiting is performed to enforce the DMP property (14) of the cell averages that define the local bounds (56). Indeed, the validity of the flux constraints (15) for H_{ij}^* defined by (12) with $\alpha_{ij} = 1$ for all $j \in \mathcal{N}_i$ does not follow from (54), although a violation of these constraints is unlikely in practice. In fact, the isotropic VB limiter tends to overconstrain u_{ih}^* . This tendency manifests itself, e.g., in the unnecessary cancellation of the solution gradients in boundary elements, where the default local bounds (56) of the inequality constraints (55) are too restrictive for $\mathbf{x}_{ip} \in \partial\Omega_h$. A possible remedy to this drawback is a customized definition of U_{ip}^{\max} and U_{ip}^{\min} for boundary vertices [1].

Another way to improve the VB limiter is to make it anisotropic, i.e., to define u_{ih}^* using the general formula (9) and choose an individual correction factor β_{ik} for each partial derivative U_{ik} . Such

anisotropic limiting approaches were explored, e.g., in [1, 24, 43]. Their disadvantages (high cost of solving inequality-constrained optimization problems or the use of closed-form approximations based on worst-case assumptions) are similar to those of slope limiting with nonlinear flux constraints. An additional disadvantage is the fact that the DMP property of cell averages needs to be assumed.

4.3. Anisotropic slope limiting under derivative constraints

The aforementioned drawbacks of anisotropic slope limiting under solution constraints of the form (54) are due to the fact that the pointwise value of u_{ih}^* at each vertex \mathbf{x}_{ip} , $p = 1, \dots, N$ depends on d correction factors $\beta_{i1}, \dots, \beta_{id}$. Hence, it is impossible to determine the optimal value of any β_{ik} without taking the other correction factors into account. To avoid this problem, we introduce a slope limiter which constrains each directional derivative $U_{ik}^* = \frac{\partial u_{ih}^*}{\partial x_k} = \beta_k \frac{\partial u_{ih}}{\partial x_k}$, $k = 1, \dots, d$ using individually chosen bounds U_{ik}^{\max} and U_{ik}^{\min} . Instead of constructing them in a way which would guarantee the DMP property for pointwise solution values and/or cell averages, we define

$$U_{ik}^{\max} = \max_{j \in \mathcal{J}_{ik}} U_{jk}^R, \quad U_{ik}^{\min} = \min_{j \in \mathcal{J}_{ik}} U_{jk}^R \quad (57)$$

using low-order reconstructed values U_{jk}^R . By default, the bounding stencil \mathcal{J}_{ik} contains the indices of all common-vertex neighbors of K_i . However, the use of individually chosen stencils for certain partial derivatives may be appropriate for anisotropic transport problems (see Section 6.1).

In contrast to finite volume and reconstruction-based DG schemes in which accurate reconstruction of derivatives from cell averages is required, a rough approximation U_{jk}^R to $\frac{\partial u}{\partial x_k}$ in K_j is sufficient to construct reasonable bounds for anisotropic slope limiting. In view of the fact that

$$\nabla u_{ih}|_{K_i} = \frac{1}{|K_i|} \sum_{j \in \mathcal{N}_i} \int_{S_{ij}} u_{ih} \mathbf{n}_{ij} \, ds \quad \forall u_{ih} \in \mathbb{P}_1(K_i) \quad (58)$$

by the divergence theorem, the simple formula

$$(U_{i1}^R, \dots, U_{id}^R)^T = \frac{1}{|K_i|} \sum_{j \in \mathcal{N}_i} \int_{S_{ij}} \left(\frac{U_{j0} + U_{i0}}{2} \right) \mathbf{n}_{ij} \, ds \quad (59)$$

can be used to calculate the approximate derivatives U_{jk}^R , $j \in \mathcal{J}_{ik}$ that define the local bounds (57).

The inequality constraints of our new slope limiting procedure are formally defined by

$$\min\{0, U_{ik}^{\min}\} \leq U_{ik}^* = \beta_k U_{ik} \leq \max\{0, U_{ik}^{\max}\}. \quad (60)$$

In practice, we calculate the components U_{ik}^* of the slope-limited gradient directly as follows:

$$U_{ik}^* = \begin{cases} \min\text{mod}(U_{ik}, U_{ik}^{\max}) & \text{if } U_{ik} > 0, \\ 0 & \text{if } U_{ik} = 0, \\ \min\text{mod}(U_{ik}, U_{ik}^{\min}) & \text{if } U_{ik} < 0. \end{cases} \quad (61)$$

The minmod function that we use in this formula is given by

$$\text{minmod}(a, b) = \begin{cases} \min\{a, b\} & \text{if } a > 0, b > 0, \\ \max\{a, b\} & \text{if } a < 0, b < 0, \\ 0 & \text{otherwise.} \end{cases} \quad (62)$$

Remark 6. The bound-preserving moment limiter proposed by Giuliani and Krivodonova [12, 13] is also based on a comparison of directional derivatives to suitably defined reconstructions from cell averages. However, our anisotropic slope limiter (61) is much simpler, especially in 3D. This simplicity is a consequence of the fact that we no longer attempt to enforce the DMP constraints (14) for cell averages in the process of slope limiting. In our last new method, these constraints are enforced using the flux limiters presented in Section 3. The purpose of slope limiting based on (60) is to ensure that the difference between U_{ik}^* and the inaccurate but consistent reconstruction (59) of the corresponding partial derivative from well-behaved BP cell averages cannot become unacceptably large.

Remark 7. The derivative constraints (60) are far less restrictive than the solution constraints (54) of the isotropic VB slope limiter. For that reason, we do not recommend the use of (61) without flux limiting. The flux limiter should be applied at each SSP Runge-Kutta stage but slope limiting via (61) may be performed just once per time step or even less frequently. Hence, the combined cost of flux and slope limiting may, in fact, be lower than that of a more sophisticated slope limiter.

Remark 8. When it comes to visualization or to computation of derived quantities which requires the validity of solution constraints (54), the isotropic VB limiter (55) may be invoked to enforce these constraints. The result will be provably BP since the DMP property of cell averages is guaranteed by the flux limiter. The original values (61) of the directional derivatives should be used in further computations (if any) because the VB postprocessing may introduce additional numerical errors.

4.4. Monolithic anisotropic slope limiting

All slope limiters presented so far were designed to directly adjust the partial derivatives U_{ik} of a given DG approximation u_{ih} . Such predictor-corrector approaches tend to cause convergence problems at steady state. Since the solution constraints (54) and derivative constraints (60) do not imply the DMP property of the cell averages, it is not necessary to enforce these constraints exactly in our method. If the fully discrete counterpart of (8) is used as a fixed-point iteration for solving a stationary hyperbolic problem, the difference between U_{ik} and U_{ik}^* can be penalized as follows:

$$\begin{aligned} & \int_{K_i} w_{ih}(u_{ih}^{\text{SSP}} - u_{ih}) \, d\mathbf{x} - \Delta t \int_{K_i} \nabla w_{ih} \cdot \mathbf{f}(u_{ih}) \, d\mathbf{x} \\ & + \Delta t \sum_{j \in \mathcal{N}_i} \int_{S_{ij}} w_{ih} [\alpha_{ij} H(u_{ih}, u_{jh}, \mathbf{n}_{ij}) + (1 - \alpha_{ij}) H_{ij}^{\mathbb{P}^0}] \, ds \\ & + \gamma \Delta t \left[\int_{K_i} (w_{ih} - W_{i0})(u_{ih}^{\text{SSP}} - U_{i0}^{\text{SSP}}) \, d\mathbf{x} - \int_{K_i} (w_{ih} - W_{i0})(u_{ih}^* - U_{i0}) \, d\mathbf{x} \right] = 0, \quad (63) \end{aligned}$$

where $\gamma > 0$ is a large penalty parameter, u_{ih} is the solution at the beginning of the time step or SSP Runge-Kutta stage, u_{ih}^* is a slope-limited approximation to u_{ih} , and α_{ij} is a flux correction factor that enforces (14) for the cell average U_{i0}^* of the updated solution u_{ih}^{SSP} . Importantly, the addition of the penalization term does not change the evolution equation for U_{i0}^* which corresponds to $w_{ih} \equiv 1$.

Remark 9. The implicit treatment of the term depending on $u_{ih}^{\text{SSP}} - U_{i0}^{\text{SSP}}$ corresponds to a diagonal correction of the element mass matrix in DG schemes using the Taylor basis (cf. [31]).

If flux limiting is performed using formula (23) with the MCL bounds (24),(25), the nonlinear discrete problem defined by (63) has a well-defined residual and steady-state solutions are independent of the pseudo-time step Δt . In Section 6.3, we use (63) as a fixed-point iteration method.

5. Entropy stabilization

In the case of a nonlinear conservation law, additional corrections may need to be performed to ensure entropy stability. A convex function $\eta : \mathbb{R} \rightarrow \mathbb{R}$ is called an entropy and $v(u) = \eta'(u)$ is called an entropy variable if there exists an entropy flux $\mathbf{q} : \mathbb{R} \rightarrow \mathbb{R}^d$ such that $v(u)\mathbf{f}'(u) = \mathbf{q}'(u)$. A weak solution u of (1) is called an entropy solution if the entropy inequality

$$\frac{\partial \eta}{\partial t} + \nabla \cdot \mathbf{q}(u) \leq 0 \quad (64)$$

holds for any entropy pair (η, \mathbf{q}) . For any smooth weak solution, the conservation law

$$\frac{\partial \eta}{\partial t} + \nabla \cdot \mathbf{q}(u) = 0 \quad (65)$$

can be derived from (1) using multiplication by the entropy variable v , the chain rule, and the definition of an entropy pair. Hence, entropy is conserved in smooth regions and dissipated at shocks.

A discretization of (1) is called entropy stable if it satisfies a (semi-)discrete version of the entropy inequality (64). In the present work, we enforce this property using the entropy correction tools developed in [31]. The underlying design criteria impose the following additional constraints:

- The limited fluxes H_{ij}^* defined by (12) should satisfy the entropy stability condition

$$(V_{j0} - V_{i0})H_{ij}^* \leq \mathbf{n}_{ij} \cdot (\boldsymbol{\psi}(U_{j0}) - \boldsymbol{\psi}(U_{i0})), \quad (66)$$

where $\boldsymbol{\psi}(u) = v(u)\mathbf{f}(u) - \mathbf{q}(u)$ and $V_{i0} = \eta'(U_{i0})$ is an approximation to the entropy variable.

- The entropy production by solution gradients should be penalized using a stabilization term

$$Q_i(w_{ih}, v_{ih}) = \nu_i \int_{K_i} (w_{ih} - W_{i0}, v_{ih} - V_{i0}) \, d\mathbf{x} \geq 0 \quad (67)$$

such that

$$P_i(v_{ih}, u_{ih}) + \sum_{j \in \mathcal{N}_i} |S_{ij}| G_{ij}^* \leq Q_i(v_{ih}, v_{ih}), \quad (68)$$

where $P_i(v_{ih}, u_{ih}) \approx \int_{K_i} \frac{\partial \eta(u)}{\partial t} d\mathbf{x}$ is the rate of entropy production in cell K_i and

$$G_{ij}^* = \frac{V_{j0} + V_{i0}}{2} H_{ij}^* - \frac{1}{2} (\psi(U_{j0}) + \psi(U_{i0})) \cdot \mathbf{n}_{ij} \quad (69)$$

is a consistent approximation to the averaged entropy flux $\frac{1}{|S_{ij}|} \int_{S_{ij}} \mathbf{q}(u) \cdot \mathbf{n}_{ij} ds$.

Note that the entropy dissipative term $Q_i(w_{ih}, v_{ih})$ exhibits the same structure as the penalization terms that we used in (63) for monolithic slope limiting. To avoid severe time step restrictions, we treat $Q_i(w_{ih}, v_{ih})$ implicitly. In the case of a general convex entropy $\eta(u) \neq \frac{u^2}{2}$, the need for solving nonlinear systems is avoided by exploiting the linearized relationship

$$V_{ik} = \eta''(U_{i0}) U_{ik}, \quad k = 1, \dots, d$$

between the partial derivatives of the conserved quantities and entropy variables, see [31].

As shown by Chen and Shu [7], the validity of (66) is guaranteed for the low-order LLF flux $H_{ij}^* = H_{ij}^{\mathbb{P}_0}$. Hence, this condition can always be satisfied by reducing the value of $\alpha_{ij} \in [0, 1]$ in (12) if necessary. In the case $v_{ih} = V_{i0}$, condition (68) holds for $Q_i(v_{ih}, v_{ih}) = 0$. For $v_{ih} \neq V_{i0}$, the entropy dissipation rate $Q_i(v_{ih}, v_{ih})$ is strictly positive and the validity of (68) can always be enforced by choosing ν_i sufficiently large. For details regarding the definition of entropy stability preserving flux correction factors α_{ij} and slope penalization parameters ν_i , we refer the interested reader to [31].

6. Numerical examples

In this section, we study the numerical behavior of different slope limiters for DG- \mathbb{P}_1 schemes. In our description of the numerical results, the methods under investigation are labeled as follows:

- FC-L: flux-constraining slope limiter (40) for linear advection, no flux limiting;
- FC-N: flux-constraining slope limiter (47) for nonlinear problems, no flux limiting;
- SC: solution-constraining vertex-based slope limiter (55), no flux limiting;
- DC: derivative-constraining anisotropic slope limiter (61) + MCL flux limiter;
- DC-M: monolithic version (63) of the slope limiter (61) + MCL flux limiter.

A comparative study of FCT and MCL flux limiters can be found in [33]. For a comparison of the SC approach to other slope limiting techniques, we refer the reader to Beisiegel [4].

All figures of this section visualize the results obtained on a mesh of square cells with uniform spacing $h = \frac{1}{128}$. Numerical solutions are advanced in (pseudo-)time using the explicit third-order three-stage

SSP Runge-Kutta method [14] and time steps satisfying condition (29). The FC-X and SC slope limiters, as well as the MCL flux limiter and the monolithic version of the DC slope limiter, are applied after each Runge-Kutta stage. The non-monolithic DC slope limiter is applied at the beginning of each time step. Before calculating the error norms and visualizing the results, we apply the SC limiter. This postprocessing constrains the output of all schemes to be in bounds not only at the centroids but also at the vertices of mesh cells. For visualization purposes, we project the postprocessed DG- \mathbb{P}_1 solutions into the space of continuous bilinear finite elements using the lumped-mass L^2 projection.

6.1. Anisotropic advection test

In the first numerical example, we solve the time-dependent linear advection equation

$$\frac{\partial u}{\partial t} + \nabla \cdot (\mathbf{v}u) = 0 \quad (70)$$

in $\Omega = (0, 1)^2$ using $\mathbf{v}(x, y) = (0, 1)$. The initial profile displayed in Fig. 1(a) is defined by [1]

$$u_0(x, y) = w(x)4y(1 - y), \quad (71)$$

where

$$w(x) = \begin{cases} 2 & \text{if } 0.2 \leq x \leq 0.4, \\ 1 & \text{otherwise.} \end{cases} \quad (72)$$

The challenge of this test is to obtain approximations which are not only DMP-satisfying but also monotonicity-preserving and do not limit the smooth derivatives $U_{i2} = \frac{\partial u_{ih}}{\partial y}$ in boundary elements. This example is specifically designed to show that isotropic limiters may produce inaccurate results in applications to anisotropic transport problems such as advection of salinity in ocean flows.

In this experiment, the local bounds (20) of the FC-L slope limiter are defined using cell average data of all common-vertex neighbors, whereas the bounding stencil \mathcal{J}_{i0} of the DC flux limiter is chosen to include only neighbors belonging to the same horizontal layer of mesh cells. The bounding stencils \mathcal{J}_{i1} and \mathcal{J}_{i2} of the DC slope limiter for partial derivatives w.r.t. $x_1 := x$ and $x_2 := y$ are defined using the horizontal and vertical neighbors, respectively. This choice is motivated by the anisotropic structure of the exact solution and exploits the option of anisotropic limiting in the DC algorithm.

Snapshots of slope-limited DG- \mathbb{P}_1 solutions obtained at $T = 0.4$ using the time step $\Delta t = 10^{-3}$ are presented in Fig. 1. All of them satisfy the inequality constraints of the underlying limiting procedures, and the cell averages stay in the range determined by the maxima and minima of the initial data. However, the FC-L and SC solutions are not monotonicity-preserving because they were obtained using multidimensional slope limiters with isotropic bounds. The local bounds of the FC-L method are wider than those of the vertex-based SC limiter, which results in larger undershoots/overshoots around the discontinuities. The anisotropic bounds of the DC method, and the way in which it constrains the directional derivatives, make it possible to preserve monotonicity along the grid lines. In Fig. 2 we compare the solution profiles produced by the methods under investigation along the line $y = 0.1$. The DC solution is perfectly monotone because the anisotropic bounds are tight and the directional derivatives are limited separately. The isotropic FC-L and SC slope limiters fail to preserve the 1D structure of the exact solution along the grid lines because the magnitude of the vertical gradient affects the bounds for variations of cell averages in the horizontal direction and vice versa.

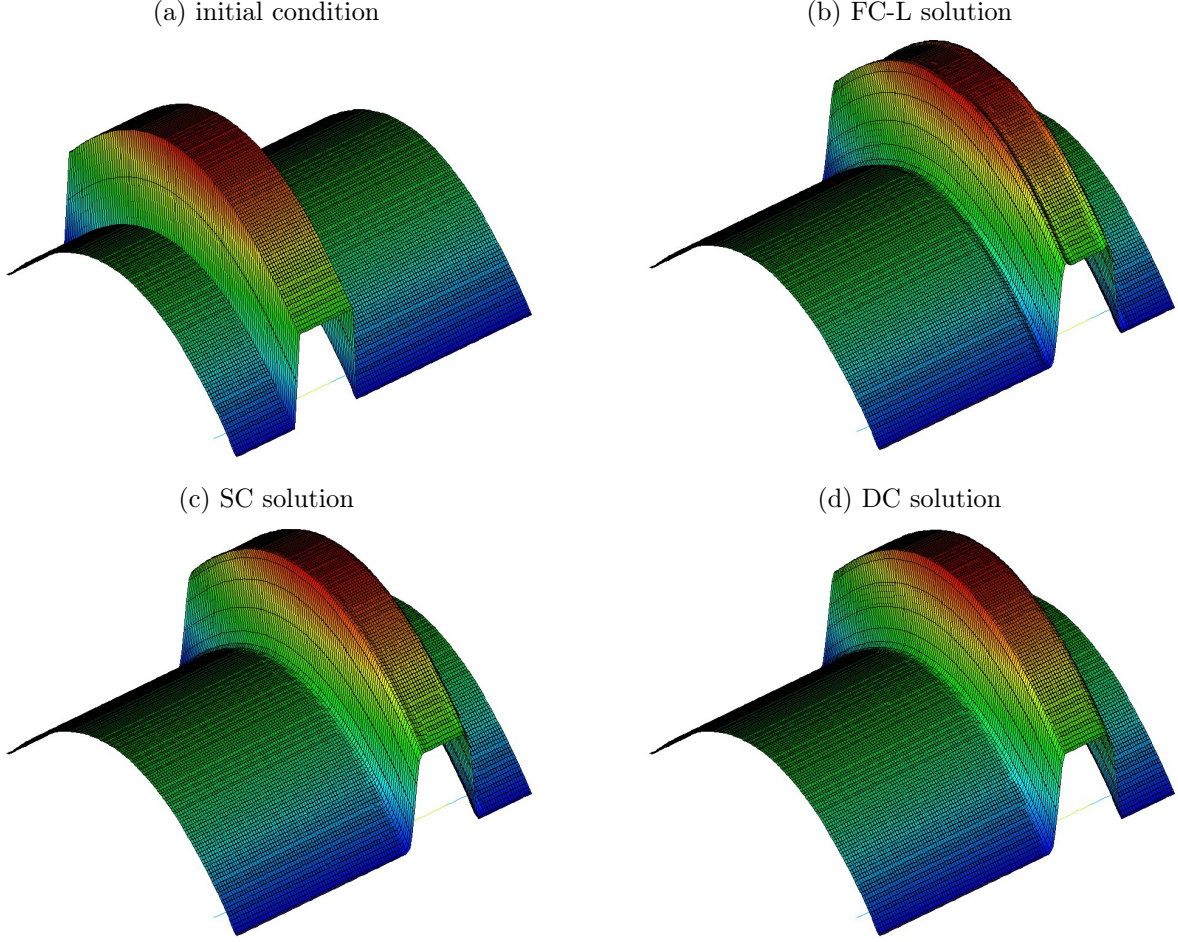


Figure 1: Anisotropic advection test. The diagrams show (a) initial data and (b)-(d) numerical solutions at $T = 0.4$ obtained with slope-limited DG- \mathbb{P}_1 methods using $h = \frac{1}{128}$ and $\Delta t = 10^{-3}$.

6.2. Solid body rotation

In the second linear advection test, we solve (70) in $\Omega = (0, 1)^2$ using the rotating velocity field $\mathbf{v}(x, y) = (0.5 - y, x - 0.5)^\top$. The initial condition, as defined by LeVeque [39], is given by

$$u_0(x, y) = \begin{cases} u_0^{\text{hump}}(x, y) & \text{if } \sqrt{(x - 0.25)^2 + (y - 0.5)^2} \leq 0.15, \\ u_0^{\text{cone}}(x, y) & \text{if } \sqrt{(x - 0.5)^2 + (y - 0.25)^2} \leq 0.15, \\ 1 & \text{if } \left(\sqrt{(x - 0.5)^2 + (y - 0.75)^2} \leq 0.15 \right) \wedge \\ & (|x - 0.5| \geq 0.025 \vee y \geq 0.85), \\ 0 & \text{otherwise,} \end{cases}$$

where

$$u_0^{\text{hump}}(x, y) = \frac{1}{4} + \frac{1}{4} \cos \left(\frac{\pi \sqrt{(x - 0.25)^2 + (y - 0.5)^2}}{0.15} \right), \quad (73)$$

$$u_0^{\text{cone}}(x, y) = 1 - \frac{\sqrt{(x - 0.5)^2 + (y - 0.25)^2}}{0.15}. \quad (74)$$

Homogeneous Dirichlet boundary conditions are prescribed on portions of $\partial\Omega$ where $\mathbf{v} \cdot \mathbf{n} < 0$.

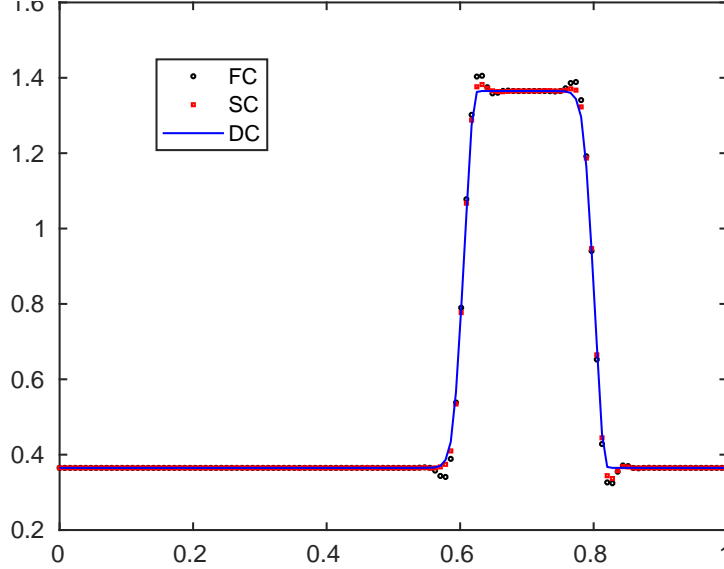
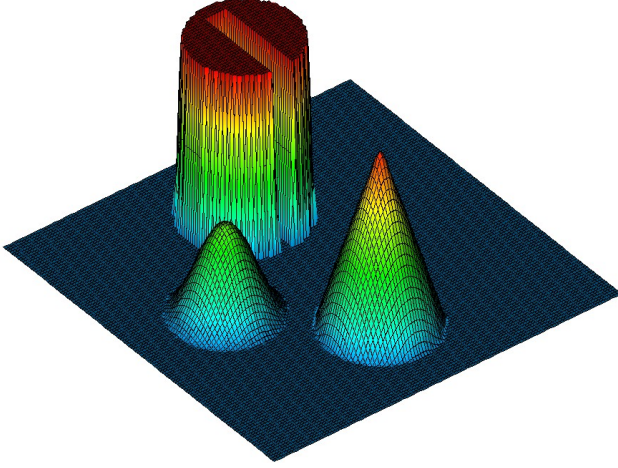


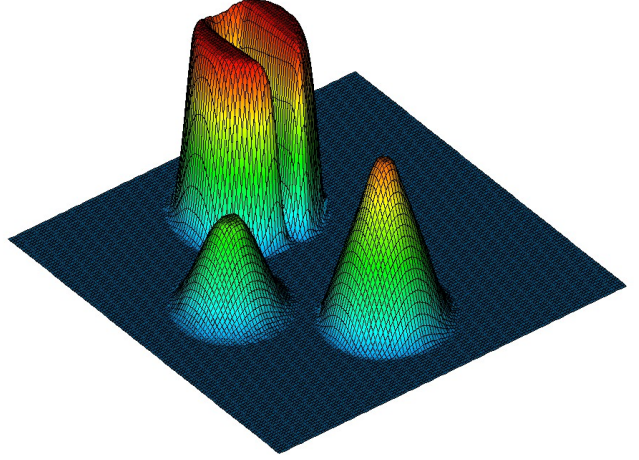
Figure 2: Anisotropic advection test. Slope-limited DG- \mathbb{P}_1 solutions at $T = 0.4$ along the line $y = 0.1$.

After each full rotation, the exact solution $u(\cdot, 2\pi k)$, $k \in \mathbb{N}$ coincides with the initial data u_0 . Numerical solutions are evolved using the time step $\Delta t = 10^{-3}$. In this example and in the remaining test runs of this section, we use isotropic bounding stencils \mathcal{J}_{ik} , $k = 0, 1, 2$ not only for the FC-L limiter but also for the DC version. The initial data and numerical results produced by the three methods after one full rotation, i.e., at the final time $T = 2\pi$, are shown in Fig. 3. The differences between the numerical solutions are not as pronounced as in the first example. The values of the global maxima listed above each plot indicate that the most diffusive approximation is produced by the vertex-based SC limiter (which in turn is far less diffusive than many other limiters for DG schemes, cf. [4]). The new FC-L and DC approaches impose DMP constraints on cell averages (rather than solution values at the vertices) using local bounds corresponding to the maximum and minimum of the SC bounds at the corners of the cell. This limiting strategy results in better preservation of the initial profile. In particular, the DC version captures the smooth peak remarkably well for a method that does not use smoothness indicators to relax the local bounds. Moreover, the FC-L and DC methods are provably bound-preserving. The SC limiter does not produce any undershoots or overshoots in this particular test but it does not generally guarantee the BP property as long as the flux limiter is deactivated.

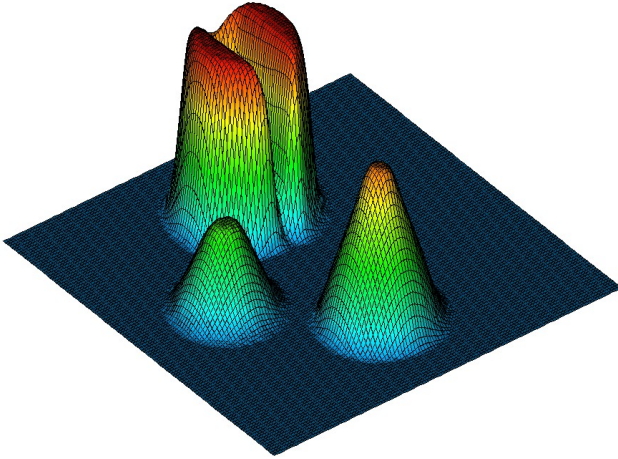
(a) exact solution, $u_h \in [0.0, 1.0]$



(b) FC-L solution, $u_h \in [0.0, 0.9995]$



(c) SC solution, $u_h \in [0.0, 0.9956]$



(d) DC solution, $u_h \in [0.0, 0.9998]$

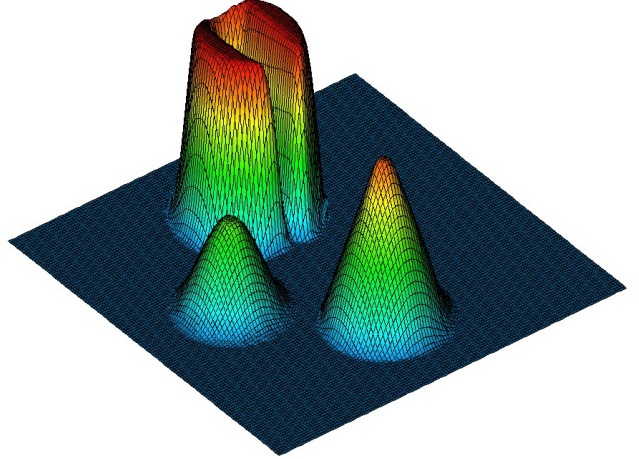


Figure 3: Solid body rotation test [39]. The diagrams show (a) exact solution / initial data and (b)-(d) numerical solutions at $T = 2\pi$ obtained with slope-limited DG- \mathbb{P}_1 methods using $h = \frac{1}{128}$ and $\Delta t = 10^{-3}$.

6.3. Steady circular advection

In the last linear advection test, we calculate steady-state solutions to (70) in $\Omega = (0, 1)^2$ using $\mathbf{v}(x, y) = (y, -x)$. The inflow boundary condition and the exact solution are given by

$$u(x, y) = \begin{cases} 1, & \text{if } 0.15 \leq r(x, y) \leq 0.45, \\ \cos^2\left(10\pi \frac{r(x, y) - 0.7}{3}\right), & \text{if } 0.55 \leq r(x, y) \leq 0.85, \\ 0, & \text{otherwise,} \end{cases} \quad (75)$$

where $r(x, y) = \sqrt{x^2 + y^2}$ is the distance to the corner point $(0, 0)$ of the unit square domain.

Numerical solutions are marched to the steady state with the same explicit SSP Runge-Kutta scheme that we use for time-dependent problems. The methods under investigation are FC-L, SC, and DC-M. The parameter γ for the penalty term of the monolithic DC scheme (63) is chosen to be $10^3 \cdot M_i$, where M_i is a diagonal entry of the Taylor mass matrix (see [30, 31] for the definition of the Taylor basis). In our experience, the DC-M results are quite insensitive to the choice of γ because the main bound-preserving correction tool of this method is the MCL flux limiting procedure.

Computations are terminated when the L^1 norm of the difference $U_{i0}^* - U_{i0}$ becomes smaller than the prescribed tolerance 10^{-10} at the first SSP RK stage of the pseudo-time step. We remark that we were often unable to reach this tolerance with the SC approach. It is widely known that SC-like limiters may inhibit convergence to steady-state solutions. The monolithic FC-L and DC-M schemes have well-defined residuals and, therefore, exhibit better steady state convergence behavior.

The exact solution (75) and numerical solutions obtained with the three methods are displayed in Fig. 4. For a better quantitative comparison, we list the L^2 errors in the approximation of cell averages (denoted by E_2) above each plot. The FC-L and DC-M errors are virtually the same, while the SC error is slightly larger due to more restrictive inequality constraints. All solutions are bounded by the maximum $u^{\max} = 1$ and minimum $u^{\min} = 0$ of the Dirichlet boundary data. No spurious oscillations are observed in the neighborhood of discontinuities, and smooth portions of the exact solution are reproduced very well. To study the numerical behavior of the three limiting techniques for a steady advection test with a globally smooth exact solution, we perform grid convergence studies for [40]

$$u(x, y) = \exp\left(-100(r(x, y) - 0.7)^2\right), \quad 0 \leq x, y \leq 1 \quad (76)$$

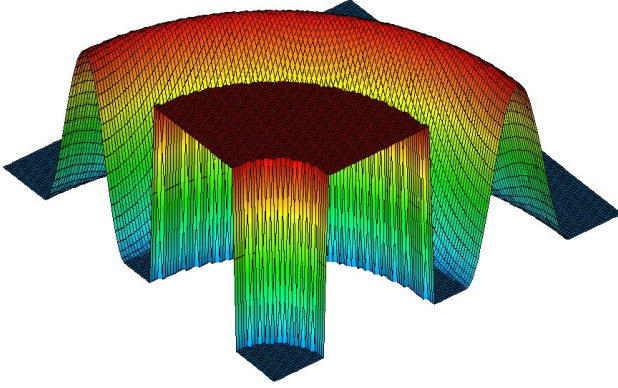
using the same velocity field. In Table 1, we present the E_2 convergence history for the standard DG- \mathbb{P}_0 method and its slope-limited counterparts. The experimental order of convergence (EOC) is above 2.0 if no limiting is performed and approximately 1.75 otherwise. Further improvements can be achieved by using less restrictive bounds, as proposed in [37]. The remarkably similar convergence behavior of the FC-L and DC schemes and the larger absolute errors of the SC method indicate that the choice of the local bounds has a stronger impact on the accuracy of slope-limited approximations to smooth solutions than the way in which these bounds are enforced in our methods.

6.4. KPP problem

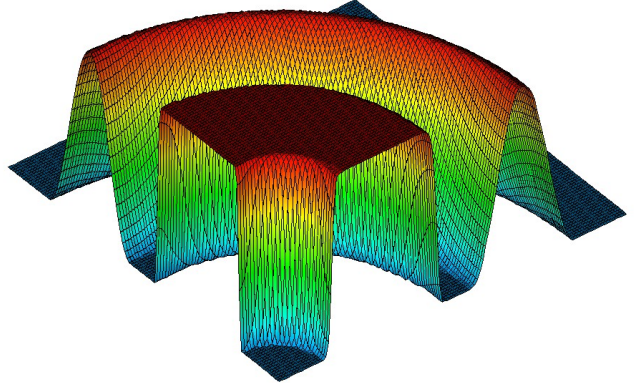
The KPP problem [18, 19, 29] is a challenging nonlinear test for verification of entropy stability properties. In this last example, we solve (1) in $\Omega = (-2, 2) \times (-2.5, 1.5)$ using the flux function

$$\mathbf{f}(u) = (\sin(u), \cos(u)) \quad (77)$$

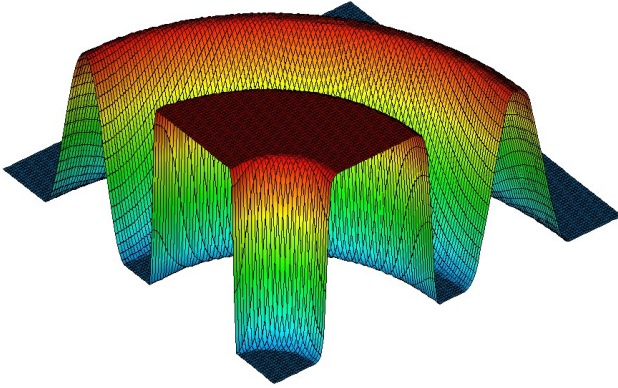
(a) exact solution, $E_2=0.000\text{e}0$



(b) FC-L solution, $E_2=0.397\text{e-}01$



(c) SC solution, $E_2=0.415\text{e-}01$



(d) DC-M solution, $E_2=0.396\text{e-}01$

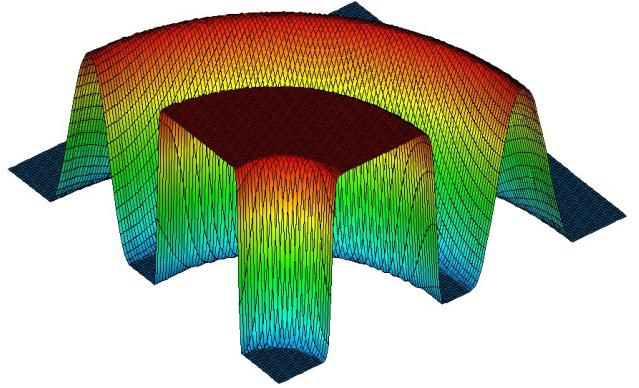


Figure 4: Steady circular advection test [32, 33]. The diagrams show (a) exact solution and (b)-(d) numerical solutions obtained with slope-limited DG- \mathbb{P}_1 methods using $h = \frac{1}{128}$.

h	$E_2^{\mathbb{P}_1}$	EOC	E_2^{FC}	EOC	E_2^{SC}	EOC	E_2^{DC}	EOC
$\frac{1}{32}$	7.17e-3		1.39e-2		3.28e-2		1.38e-2	
$\frac{1}{64}$	1.68e-3	2.09	4.02e-3	1.79	1.04e-2	1.66	4.00e-2	1.79
$\frac{1}{128}$	4.09e-4	2.04	1.20e-3	1.75	3.00e-3	1.79	1.20e-3	1.74
$\frac{1}{256}$	1.01e-4	2.02	3.59e-4	1.74	8.30e-4	1.85	3.59e-4	1.74

Table 1: Convergence behavior of the DG- \mathbb{P}_1 methods in steady-state computations for the steady circular advection test with the smooth inflow profile (76).

and the initial condition

$$u_0(x, y) = \begin{cases} \frac{14\pi}{4} & \text{if } \sqrt{x^2 + y^2} \leq 1, \\ \frac{\pi}{4} & \text{otherwise.} \end{cases} \quad (78)$$

The entropy flux corresponding to $\eta(u) = \frac{u^2}{2}$ is $\mathbf{q}(u) = (u \sin(u) + \cos(u), u \cos(u) - \sin(u))$. The exact solution exhibits a two-dimensional rotating wave structure which is difficult to capture correctly.

We define the LLF flux (3) using the global upper bound $\lambda^{\max} = 1$ for the maximum wave speed. More accurate estimates can be found in [19]. In our numerical study of the FC-N, SC, and DC methods for the KPP problem, we use the entropy correction tools outlined in Section 5 in addition to bound-preserving flux/slope limiting. Snapshots of the numerical solutions at the final time $T = 1.0$ are presented in Figs. 5 and 6. The diffusive DG- \mathbb{P}_0 results are included to illustrate the correct wave structure of the entropy solution. As noticed by Guermond et al. [18], high-order finite element schemes may converge to wrong weak solutions of the KPP problem even if they are equipped with bound-preserving limiters. None of our entropy-stabilized DG- \mathbb{P}_1 methods exhibits this behavior. The twisted shocks stay clearly separated, while the levels of numerical dissipation are reduced compared to DG- \mathbb{P}_0 . The sharpest resolution of discontinuities is obtained with our DC approach. The new FC-N limiter performs better than the SC limiter. These encouraging results demonstrate that the DMP property and entropy stability of a slope-limited DG- \mathbb{P}_1 approximation can be guaranteed using fairly simple limiting techniques which are at least as robust and accurate as existing alternatives.

7. Conclusions

The findings reported in this work reveal some interesting relationships between flux and slope limiting in DG- \mathbb{P}_1 methods for hyperbolic problems. In particular, it turns out that a carefully designed slope limiter can act as a flux limiter, i.e., provably enforce flux constraints which imply a discrete maximum principle for cell averages. However, our preferred limiting strategy is a combination of flux correction for cell averages and slope correction for directional derivatives. We have shown that this approach makes it possible to cure some alarming deficiencies of existing limiting techniques. We also discussed the design of anisotropic and monolithic limiters in this framework. Last but not least, we addressed the aspects of entropy stabilization via flux limiting and slope penalization.

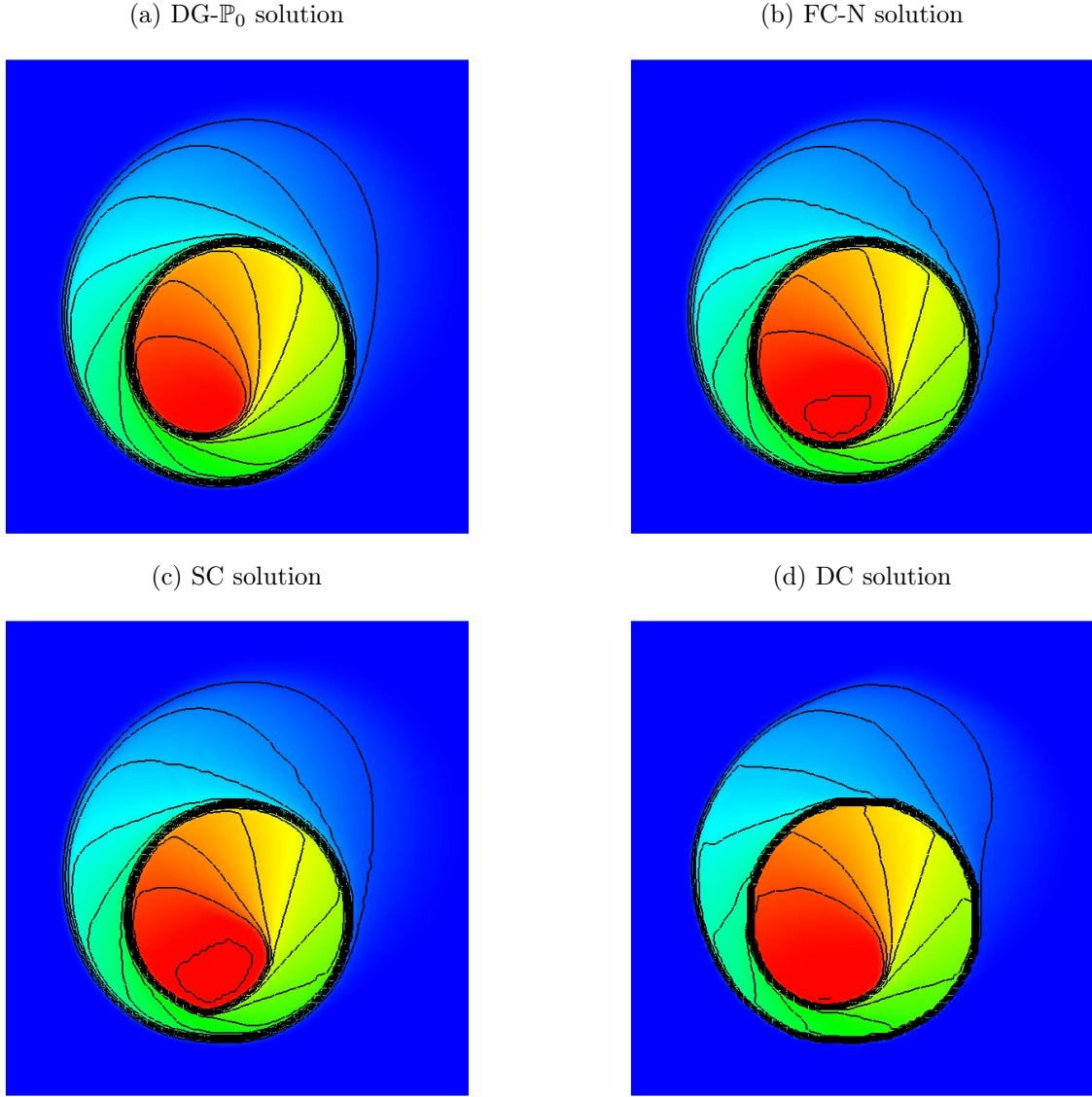


Figure 5: KPP problem [29]. The 2D plots show (a) property-preserving DG- \mathbb{P}_0 solution and (b)-(d) entropy-stabilized slope-limited DG- \mathbb{P}_1 solutions at $t = 1.0$ obtained with $h = \frac{1}{128}$ and $\Delta t = 10^{-3}$.

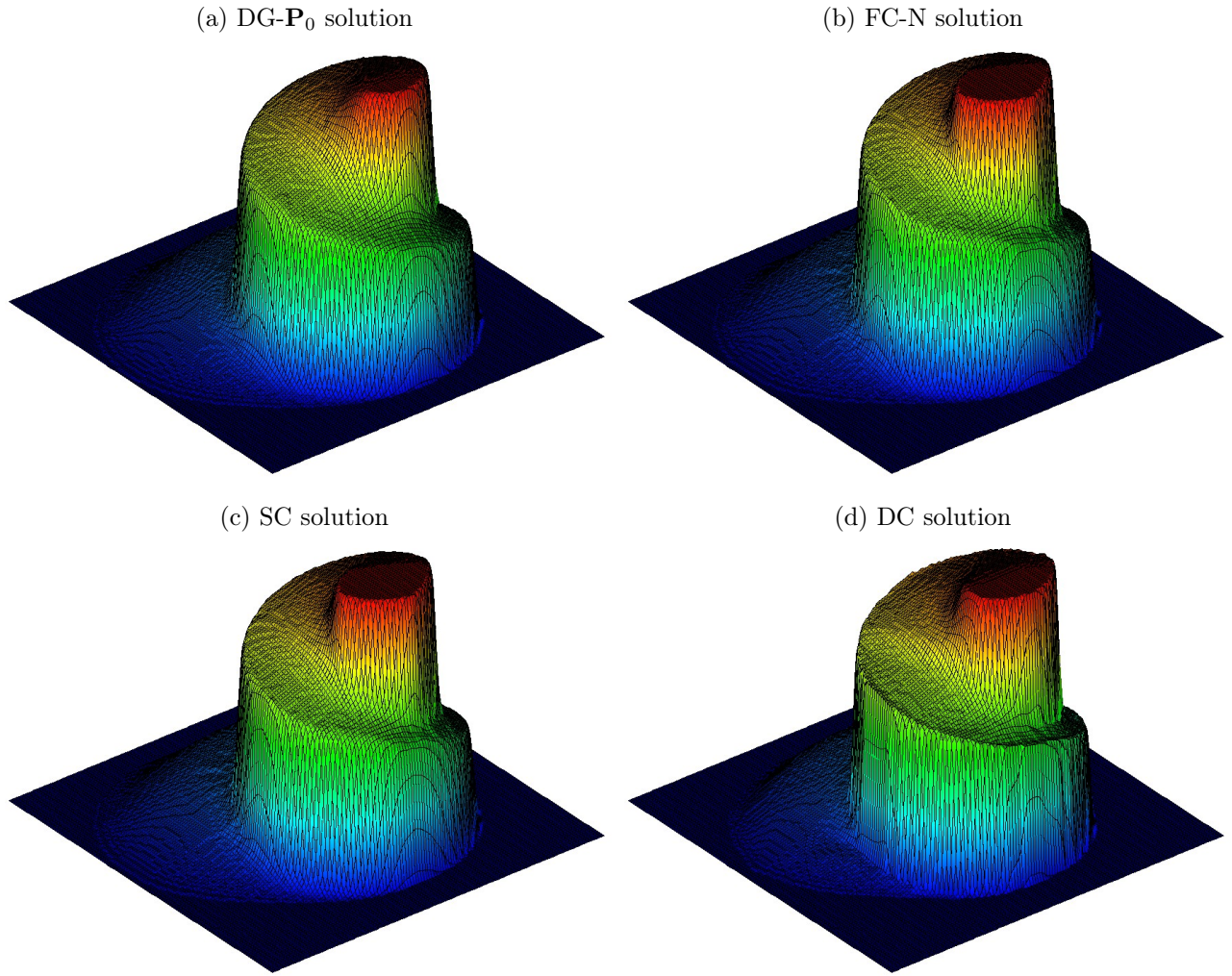


Figure 6: KPP problem [29]. The 3D plots show (a) property-preserving DG- \mathbb{P}_0 solution and (b)-(d) entropy-stabilized slope-limited DG- \mathbb{P}_1 solutions at $T = 1.0$ obtained with $h = \frac{1}{128}$ and $\Delta t = 10^{-3}$.

The FCT and MCL flux limiters presented in this work have already been extended to nonlinear hyperbolic systems and guarantee preservation of invariant domains [16, 17, 20, 32, 45]. Extensions to high-order finite element approximations and general high-order Runge-Kutta methods are feasible as well. In principle, the methodology proposed in the present paper is directly applicable to finite elements of arbitrary order. However, recent advances in the development of algebraic limiting approaches [20, 21, 34, 35, 36, 42, 45] indicate that a localization to subcells is required to achieve at least the same accuracy as with the DG- \mathbb{P}_1 scheme using the same number of degrees of freedom. The simplest way to meet this requirement is to construct an *hp*-adaptive partition of unity for the pair of finite

element spaces corresponding to a high-order DG method and the DG- \mathbb{P}_1 subcell approximation on a submesh with the same nodes [36]. Using a smoothness indicator to select the appropriate local basis in each cell, the application of limiters can be restricted to \mathbb{P}_1 subcells without losing the high accuracy of the DG approximation elsewhere. To preserve the high accuracy and DMP property of the space discretization, time integration may need to be performed using a flux-corrected Runge-Kutta method of sufficiently high order. The first representatives of such methods were recently developed in [37, 42]. In summary, the proposed methodology can be extended to high-order space-time discretizations but many additional aspects must be taken into account to reap the potential benefits.

References

- [1] V. Aizinger, A. Kosik, D. Kuzmin, and B. Reuter, Anisotropic slope limiting for discontinuous Galerkin methods. *Int. J. Numer. Methods Fluids* **84** (2017) 543-565.
- [2] T. Barth and D.C. Jespersen, The design and application of upwind schemes on unstructured meshes. *AIAA Paper*, 89-0366, 1989.
- [3] T. Barth and M. Ohlberger, Finite volume methods: foundation and analysis. In: E. Stein, R. de Borst, T.J.R. Hughes (eds), *Encyclopedia of Computational Mechanics, Volume 1: Fundamentals*. John Wiley & Sons, 2004, 439-474.
- [4] N. Beisiegel, *High-order Adaptive Discontinuous Galerkin Inundation Modeling*. PhD thesis, University of Hamburg, 2014.
- [5] J.P. Boris and D.L. Book, Flux-Corrected Transport: I. SHASTA, a fluid transport algorithm that works. *J. Comput. Phys.* **11** (1973) 38-69.
- [6] H. Burchard and H. Rennau, Comparative quantification of physically and numerically induced mixing in ocean models. *Ocean Modelling* **20** (2008) 293-311.
- [7] T. Chen and C.W. Shu, Entropy stable high order discontinuous Galerkin methods with suitable quadrature rules for hyperbolic conservation laws. *J. Comput. Phys.* **345** (2017) 427-461.
- [8] I. Christov and B. Popov, New non-oscillatory central schemes on unstructured triangulations for hyperbolic systems of conservation laws. *J. Comput. Phys.* **227-11**, (2008) 5736-5757.
- [9] B. Cockburn and C.-W. Shu, TVB Runge-Kutta local projection discontinuous Galerkin finite element method for scalar conservation laws II: General framework. *Math. Comp.* **52** (1989) 411-435.
- [10] C.J. Cotter and D. Kuzmin, Embedded discontinuous Galerkin transport schemes with localised limiters. *J. Comput. Phys.* **311** (2016) 363-373.

- [11] F. Frank, A. Rupp, and D. Kuzmin, Bound-preserving flux limiting schemes for DG discretizations of conservation laws with applications to the Cahn–Hilliard equation *Computer Methods Appl. Mech. Engrg.* **359** (2020) 112665.
- [12] A. Giuliani and L. Krivodonova. A moment limiter for the discontinuous Galerkin method on unstructured triangular meshes. *SIAM J. Sci. Comput.* **41** (2019) A508–A537.
- [13] A. Giuliani and L. Krivodonova. A moment limiter for the discontinuous Galerkin method on unstructured tetrahedral meshes. *J. Comput. Phys.* **404** (2020) 109106.
- [14] S. Gottlieb, C.-W. Shu, and E. Tadmor, Strong stability-preserving high-order time discretization methods. *SIAM Review* **43** (2001) 89–112.
- [15] S.M. Griffies, R.C. Pacanowski, and R. W. Hallberg, Spurious diapycnal mixing associated with advection in a z -coordinate ocean model. *Monthly Weather Review* **128** (2000) 538–564.
- [16] J.-L. Guermond, M. Nazarov, B. Popov, and I. Tomas, Second-order invariant domain preserving approximation of the Euler equations using convex limiting. *SIAM J. Sci. Computing* **40** (2018) A3211–A3239.
- [17] J.-L. Guermond, M. Nazarov, and I. Tomas, Invariant domain preserving discretization-independent schemes and convex limiting for hyperbolic systems. *Computer Methods Appl. Mech. Engrg.* **347** (2019) 143–175.
- [18] J.-L. Guermond and B. Popov, Invariant domains and first-order continuous finite element approximation for hyperbolic systems. *SIAM J. Numer. Anal.* **54** (2016) 2466–2489.
- [19] J.-L. Guermond and B. Popov, Invariant domains and second-order continuous finite element approximation for scalar conservation equations. *SIAM J. Numer. Anal.* **55** (2017) 3120–3146.
- [20] H. Hajduk, Monolithic convex limiting in discontinuous Galerkin discretizations of hyperbolic conservation laws. Preprint [arXiv:2007.01212v2](https://arxiv.org/abs/2007.01212v2) [[math.NA](https://arxiv.org/archive/math)], 2020.
- [21] H. Hajduk, D. Kuzmin, Tz. Kolev, V. Tomov, I. Tomas, and J.N. Shadid, Matrix-free subcell residual distribution for Bernstein finite elements: Monolithic limiting. *Computers & Fluids*. **200** (2020) 104–451.
- [22] A. Harten, High resolution schemes for hyperbolic conservation laws. *J. Comput. Phys.* **49** (1983) 357–393.
- [23] A. Harten, On a class of high resolution total-variation-stable finite-difference-schemes. *SIAM J. Numer. Anal.* **21** (1984) 1–23.
- [24] H. Hoteit, Ph. Ackerer, R. Mosé, J. Erhel, and B. Philippe, New two-dimensional slope limiters for discontinuous Galerkin methods on arbitrary meshes. *Int. J. Numer. Meth. Engrg.* **61** (2004) 2566–2593.

- [25] A. Jameson, Computational algorithms for aerodynamic analysis and design. *Appl. Numer. Math.* **13** (1993) 383–422.
- [26] A. Jameson, Analysis and design of numerical schemes for gas dynamics 1. Artificial diffusion, upwind biasing, limiters and their effect on accuracy and multigrid convergence. *Int. Journal of CFD* **4** (1995) 171–218.
- [27] L. Krivodonova, Limiters for high-order discontinuous Galerkin methods. *J. Comput. Phys.* **226** (2007) 879–896.
- [28] L. Krivodonova, J. Xin, J.-F. Remacle, N. Chevaugeon, and J.E. Flaherty, Shock detection and limiting with discontinuous Galerkin methods for hyperbolic conservation laws. *Appl. Numer. Math.* **48** (2004) 323–338.
- [29] A. Kurganov, G. Petrova, and B. Popov, Adaptive semidiscrete central-upwind schemes for non-convex hyperbolic conservation laws. *SIAM J. Sci. Comput.* **29** (2007) 2381–2401.
- [30] D. Kuzmin, A vertex-based hierarchical slope limiter for p-adaptive discontinuous Galerkin methods. *J. Comput. Appl. Math.* **233** (2010) 3077–3085.
- [31] D. Kuzmin, Entropy stabilization and property-preserving limiters for discontinuous Galerkin discretizations of nonlinear hyperbolic equations. Preprint [arXiv:2004.03521 \[math.NA\]](#), 2020.
- [32] D. Kuzmin, Monolithic convex limiting for continuous finite element discretizations of hyperbolic conservation laws. *Comput. Methods Appl. Mech. Engrg.* **361** (2020) 112804.
- [33] D. Kuzmin, H. Hajduk, and A. Rupp, Locally bound-preserving enriched Galerkin methods for the linear advection equation. *Computers and Fluids* **205** (2020) 104525.
- [34] D. Kuzmin and M. Quezada de Luna, Subcell flux limiting for high-order Bernstein finite element discretizations of hyperbolic conservation laws. *J. Comput. Phys.* **411** (2020) 109411.
- [35] D. Kuzmin and M. Quezada de Luna, Entropy conservation property and entropy stabilization of high-order continuous Galerkin approximations to scalar conservation laws. Preprint [arXiv:2005.08788 \[math.NA\]](#), 2020.
- [36] D. Kuzmin, M. Quezada de Luna, and C. Kees, A partition of unity approach to adaptivity and limiting in continuous finite element methods. *Computers & Mathematics with Applications* **78** (2019) 944–957.
- [37] D. Kuzmin, M. Quezada de Luna, D. Ketcheson, and J. Grill, Bound-preserving convex limiting for high-order Runge-Kutta time discretizations of hyperbolic conservation laws. In preparation.
- [38] R.J. LeVeque, *Numerical Methods for Conservation Laws*. Birkhäuser, 1992.

- [39] R.J. LeVeque, High-resolution conservative algorithms for advection in incompressible flow. *SIAM Journal on Numerical Analysis* **33**, (1996) 627–665.
- [40] C. Lohmann, *Physics-Compatible Finite Element Methods for Scalar and Tensorial Advection Problems*. Springer Spektrum, 2019.
- [41] C. Lohmann and D. Kuzmin, Synchronized flux limiting for gas dynamics variables. *J. Comput. Phys.* **326** (2016) 973–990.
- [42] C. Lohmann, D. Kuzmin, J.N. Shadid, and S. Mabuza, Flux-corrected transport algorithms for continuous Galerkin methods based on high order Bernstein finite elements. *J. Comput. Phys.* **344** (2017) 151–186.
- [43] S. May and M. Berger, Two-dimensional slope limiters for finite volume schemes on non-coordinate-aligned meshes. *SIAM J. Sci. Comput.* **35** (2013) A2163–A2187.
- [44] S.A. Moe, J.A. Rossmanith, and D.C. Seal, Positivity-preserving discontinuous Galerkin methods with Lax-Wendroff time discretizations. *J. Sci. Comput.* **71** (2017) 44–70.
- [45] W. Pazner, Sparse invariant domain preserving discontinuous Galerkin methods with subcell convexlimiting. Preprint [arXiv:2004.08503 \[math.NA\]](#), 2020.
- [46] S.T. Zalesak, Fully multidimensional flux-corrected transport algorithms for fluids. *J. Comput. Phys.* **31** (1979) 335–362.
- [47] S.T. Zalesak, A preliminary comparison of modern shock-capturing schemes: linear advection. In: R. Vichnevetsky and R. Stepleman (eds), *Advances in Computer Methods for PDEs*. Publ. IMACS, 1987, 15–22.
- [48] X. Zhang and C-W. Shu, On positivity-preserving high order discontinuous Galerkin schemes for compressible Euler equations on rectangular meshes. *J. Comput. Phys.* **229** (2010) 8918–8934.
- [49] X. Zhang and C-W. Shu, Maximum-principle-satisfying and positivity-preserving high-order schemes for conservation laws: survey and new developments. *Proc. R. Soc. A* **467** (2011) 2752–2776.